

Accepted Manuscript

The discovery of quinoline-3-carboxamides as hematopoietic prostaglandin D synthase (H-PGDS) inhibitors

David N. Deaton, Young Do, Jason Holt, Michael R. Jeune, H. Fritz Kramer, Andrew L. Larkin, Lisa A. Orband-Miller, Gregory E. Peckham, Chuck Poole, Daniel J. Price, Lee T. Schaller, Ying Shen, Lisa M. Shewchuk, Eugene L. Stewart, J. Darren Stuart, Stephen A. Thomson, Paris Ward, Joseph W. Wilson, Tianshun Xu, Jeffrey H. Guss, Caterina Musetti, Alan R. Rendina, Karen Affleck, David Anders, Ashley P. Hancock, Heather Hobbs, Simon T. Hodgson, Jonathan Hutchinson, Melanie V. Leveridge, Harry Nicholls, Ian E. D. Smith, Don O. Somers, Helen F. Sneddon, Sorif Uddin, Anne Cleasby, Paul N. Mortenson, Caroline Richardson, Gordon Saxty

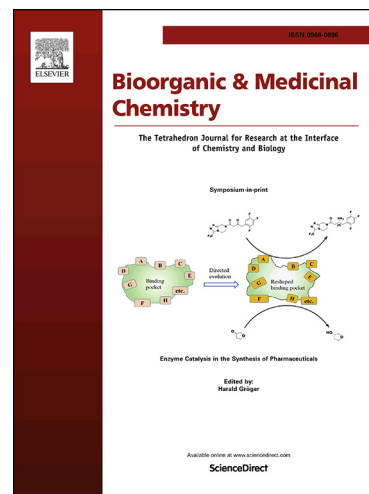
PII: S0968-0896(18)32008-X
DOI: <https://doi.org/10.1016/j.bmc.2019.02.017>
Reference: BMC 14753

To appear in: *Bioorganic & Medicinal Chemistry*

Received Date: 14 December 2018
Revised Date: 30 January 2019
Accepted Date: 8 February 2019

Please cite this article as: Deaton, D.N., Do, Y., Holt, J., Jeune, M.R., Fritz Kramer, H., Larkin, A.L., Orband-Miller, L.A., Peckham, G.E., Poole, C., Price, D.J., Schaller, L.T., Shen, Y., Shewchuk, L.M., Stewart, E.L., Darren Stuart, J., Thomson, S.A., Ward, P., Wilson, J.W., Xu, T., Guss, J.H., Musetti, C., Rendina, A.R., Affleck, K., Anders, D., Hancock, A.P., Hobbs, H., Hodgson, S.T., Hutchinson, J., Leveridge, M.V., Nicholls, H., E. D. Smith, I., Somers, D.O., Sneddon, H.F., Uddin, S., Cleasby, A., Mortenson, P.N., Richardson, C., Saxty, G., The discovery of quinoline-3-carboxamides as hematopoietic prostaglandin D synthase (H-PGDS) inhibitors, *Bioorganic & Medicinal Chemistry* (2019), doi: <https://doi.org/10.1016/j.bmc.2019.02.017>

This is a PDF file of an unedited manuscript that has been accepted for publication. As a service to our customers we are providing this early version of the manuscript. The manuscript will undergo copyediting, typesetting, and review of the resulting proof before it is published in its final form. Please note that during the production process errors may be discovered which could affect the content, and all legal disclaimers that apply to the journal pertain.



The discovery of quinoline-3-carboxamides as hematopoietic prostaglandin D synthase (H-PGDS) inhibitors

David N. Deaton,^{a,*} Young Do,^a Jason Holt,^a Michael R. Jeune,^a H. Fritz Kramer,^a Andrew L. Larkin,^a Lisa A. Orband-Miller,^a Gregory E. Peckham,^a Chuck Poole,^a Daniel J. Price,^a Lee T. Schaller,^a Ying Shen,^a Lisa M. Shewchuk,^a Eugene L. Stewart,^a J. Darren Stuart,^a Stephen A. Thomson,^a Paris Ward,^a Joseph W. Wilson,^a Tianshun Xu,^a Jeffrey H. Guss,^b Caterina Musetti,^b Alan R. Rendina,^b Karen Affleck,^c David Anders,^c Ashley P. Hancock,^c Heather Hobbs,^c Simon T. Hodgson,^c Jonathan Hutchinson,^c Melanie V. Leveridge,^c Harry Nicholls,^c Ian E. D. Smith,^c Don O. Somers,^c Helen F. Sneddon,^c Sorif Uddin,^c Anne Cleasby,^d Paul N. Mortenson,^d Caroline Richardson,^d Gordon Saxty,^d

^aGlaxoSmithKline, 5 Moore Drive, P.O. Box 13398, Research Triangle Park, NC 27709, USA

^bGlaxoSmithKline, 1250 South Collegeville Road, Collegeville, PA 19426, USA

^cGlaxoSmithKline, Gunnels Wood Road, Stevenage, Hertfordshire SG1 2NY, UK

^dAstex Pharmaceuticals, 436 Cambridge Science Park, Milton Road, Cambridge CB4 0QA, UK

*Corresponding author. E-mail address: david.n.deaton@gsk.com.

KEYWORDS: Prostaglandin D₂, PGD₂, Hematopoietic prostaglandin D synthase, H-PGDS, H-PGDS inhibitor, Fragment-based drug discovery

Abstract

With the goal of discovering more selective anti-inflammatory drugs, than COX inhibitors, to attenuate prostaglandin signaling, a fragment-based screen of hematopoietic prostaglandin D synthase was performed. The 76 crystallographic hits were sorted into similar groups, with the 3-cyano-quinoline **1a** (FP IC₅₀ = 220,000 nM, LE = 0.43) being a potent member of the 6,6-fused heterocyclic cluster. Employing SAR insights gained from structural comparisons of other H-PGDS fragment binding mode clusters, the initial hit **1a** was converted into the 70-fold more potent quinoline **1d** (IC₅₀ = 3,100 nM, LE = 0.49). A systematic substitution of the amine moiety of **1d**, utilizing structural information and array chemistry, with modifications to improve inhibitor stability, resulted in the identification of the 300-fold more active H-PGDS inhibitor tool compound **1bv** (IC₅₀ = 9.9 nM, LE = 0.42). This selective inhibitor exhibited good murine pharmacokinetics, dose-dependently attenuated PGD₂ production in a mast cell degranulation assay and should be suitable to further explore H-PGDS biology.

1.1 Introduction

The prostaglandins (PGs) are physiologically active, cyclic, oxygenated lipid compounds that are synthesized in the cell from the polyunsaturated fatty acid arachidonic acid, which is liberated from the *sn*2 position of glycerophospholipids by phospholipase A₂.¹ Cyclooxygenases 1 or 2 (COX 1 & 2, prostaglandin endoperoxide synthases 1 & 2 (PGHS1 & 2)) insert two O₂ molecules into arachidonic acid to produce prostaglandin G₂ (PGG₂), and subsequently reduce PGG₂ to PGH₂. Various synthases then convert PGH₂ into PGD₂, PGE₂, PGF_{2α}, PGI₂, and thromboxane A₂ (TxA₂). These prostanoids are then secreted by the multidrug resistance protein 4 (MRP4, ABCC4),² where they act as autocrine or paracrine factors on adjacent cells via signaling through various seven transmembrane G-protein-coupled receptors.³ They can subsequently be taken back up by cells via the prostaglandin transporter (PGT, solute carrier organic ion transporter 2A1 (SLCO2A1), organic anion transporting polypeptide 2A1 (OATO2A1))⁴ and inactivated by the enzyme 15-hydroxyprostaglandin dehydrogenase.⁵

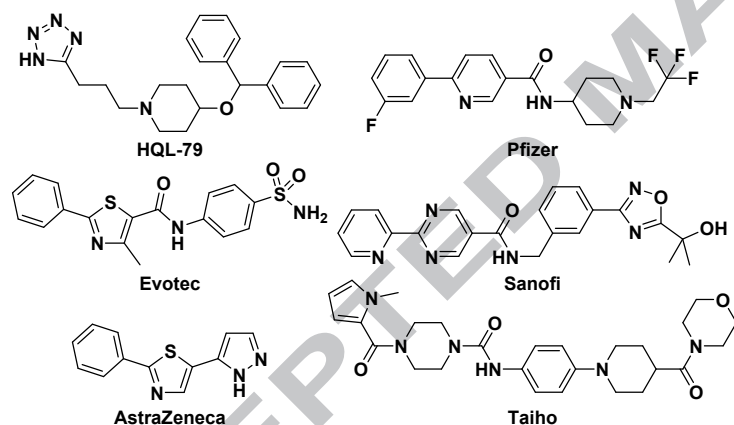
PGD₂ is produced by hematopoietic and/or lipocalin prostaglandin D synthases (EC 5.3.99.2, H-PGDS and L-PGDS) from PGH₂ by isomerization. It can be reduced by 11-keto PGD₂ reductase (aldo-keto reductase 1C3 (AKR1C3)) to 9α, 11β-PGF₂.⁶ PGD₂ can also dehydrate to form PGJ₂, Δ¹²-PGJ₂, and/or 15-deoxy-Δ^{12,14}-PGJ₂. PGD₂ signals through the seven transmembrane receptors DP₁ (G_s-coupled, stimulates cAMP production and Ca²⁺ release) and DP₂ (Chemoattractant Receptor-homologous molecule expressed on T_h2 cells receptor (CRTH2), G_i-coupled, mobilizes Ca²⁺). PGD₂ is a major prostaglandin produced by mast cells and helps mediate the inflammatory responses of type 2 helper T lymphocytes (T_h2 cells), mast cells, eosinophils, and dendritic cells. PGD₂ induces chemotaxis and stimulates cytokine production and has been implicated in allergic asthma,⁷ atopic

dermatitis,^{8,9} niacin-induced vasodilation,¹⁰ inflammatory bowel disease,¹¹ and hair growth inhibition.^{12,13} The physiological activity of PGD₂ could be selectively attenuated by either antagonizing its interaction with any or all its receptors, inhibiting either or both of its synthases, or enhancing its degradation.

H-PGDS is a member of the σ -class of glutathione-S-transferases.¹⁴ Its fellow enzyme, L-PGDS, is a member of the lipocalin gene family;¹⁵ these structurally different proteins are an example of functional convergence. Consequently, inhibitors of one enzyme may not be expected to bind to and interfere with the other enzyme's activity (*vide infra*). H-PGDS is expressed in dendritic cells and Langerhans cells of skin, Kupffer cells in the liver, dendritic cells in the thymus, microglia in the brain, the oviduct, and megakaryocytes in the bone marrow, as well as in mast cells, eosinophils, and activated T_H2 cells in many tissues. H-PGDS has been implicated in asthma,¹⁶ allergic rhinitis,¹⁷ Krabbe disease,¹⁸ Duchenne muscular dystrophy,¹⁹ and lupus.²⁰

Consequently, there has been strong interest in the discovery of H-PGDS inhibitors as potential treatments of these conditions, with several research groups, including Osaka (HQL-79),²¹ Evotec,²² AstraZeneca,²³ Pfizer,²⁴ and Sanofi (SAR191801B)²⁵ disclosing their efforts in the primary literature. There is also an excellent review of H-PGDS inhibitors from 2012.²⁶ The structures of several representative H-PGDS tool compounds are depicted in Figure 1. Recently, Taiho began a phase I clinical trial of a H-PGDS inhibitor TAS-205 in Duchenne muscular dystrophy patients.²⁷ Although, the structure of TAS-205 has not been identified, the structure may be the one shown below from a recent Taiho patent application.²⁸ With the many difficulties in translating efficacious tool compounds into safe and effective drugs in humans, multiple H-PGDS chemotypes entering clinical trials will maximize the chance for successful delivery of a medicine to aid patients with aberrant PGD₂ production, thus requiring addition efforts to identify suitable H-PGDS inhibitors for clinical investigation.

Figure 1. H-PGDS tool compounds.



As part of a larger drug discovery collaboration between GlaxoSmithKline and Astex Pharmaceuticals, a fragment-based screening approach was initiated to discover inhibitors of H-PGDS for the treatment of various inflammatory diseases.^{29,30} In comparison to high throughput screens, fragment-based screening campaigns sample chemical space more efficiently, are cheaper to screen, are simpler to triage, and often provide more drug-like starting points. This screening campaign resulted in the generation of 76 crystallographic hits, which were clustered and classified based on their protein interactions and available growth vectors for chemistry. Hits from two of these clusters were recently described.³¹ Another cluster consisting of 6,6-fused heterocycles contained the commercially available 3-cyano-quinoline **1a**. It was a weak, competitive, reversible inhibitor of H-PGDS in a fluorescence polarization assay (FP IC₅₀ = 220,000 nM), but exhibited an excellent ligand efficiency (LE = 0.43).³²

Another X-ray hit from this 6,6-fused heterocycle cluster was 8-methoxychroman-3-carbonitrile. Although synthetically less tractable, this fragment suggested that addition of an 8-methoxy moiety to quinoline **1a** might be beneficial to inhibitor potency. Furthermore, it could be inferred from another X-ray hit, 6-methoxy-1*H*-benzo[d]imidazole, from a different cluster, consisting of 5,6-fused heterocycles, which bound similarly to the quinoline **1a**, that addition of a 7-methoxy group to the quinoline hit might also enhance H-PGDS inhibition. These SAR insights gained from the binding mode clustering approach of these X-ray structures were applied to the quinoline template. The commercially available quinolines were purchased and tested. The 7- and 8-

methoxyquinoline-3-carbonitriles **1b** (FP $IC_{50} = 13,000$ nM) and **1c** (FP $IC_{50} = 5,000$ nM) were over a log more potent than nitrile **1a**. This increase in inhibitory activity led to these compounds showing activity in a RapidFire™ mass spectrometry assay measuring the inhibition of the conversion of PGH_2 , generated in situ by COX-2 from arachidonic acid, to PGD_2 by H-PGDS (**1b** ($IC_{50} = 13,000$ nM, LE = 0.49) and **1c** ($IC_{50} = 8,400$ nM, LE = 0.51)). Both compounds maintained good ligand efficiencies.

As shown in Figure 2, the co-crystal structure of fragment **1a** bound to rat H-PGDS (rH-PGDS) and glutathione (GSH) revealed that the quinoline ring forms a face to face π - π stacking interaction with the indole side chain of ^{104}Trp (face of indole ^{104}Trp to face of quinoline **1a** distance = 3.6 Å). The coplanar 3-nitrile group facilitates this interaction, withdrawing electron density from the quinoline ring and improving the interaction with the π -cloud of the indole ring. Also, the quinoline nitrogen of **1a** forms a hydrogen bond with a tightly bound, structural water molecule (structural water oxygen to quinoline nitrogen distance = 2.9 Å) that is held in place via hydrogen bonds to the C-terminal carboxylic acid of ^{199}Leu , the hydroxyl side chain of ^{159}Thr , and another bound water molecule. This binding mode is similar to the Pfizer and Sanofi series, mimicking their pyridine and pyrimidine nitrogen interactions with the protein. The 7- and 8-methoxy groups likely strengthen this interaction by increasing the basicity of the quinoline nitrogen.

Furthermore, hit to lead efforts on the chroman series showed that substituted 3-carboxamides replacements of the nitrile enhanced potency and these learnings were utilized in the quinoline series. As shown in Table 1, the 7-methoxy-*N*-methylquinoline-3-carboxamide **1d** ($IC_{50} = 3,100$ nM, LE = 0.49) was a 4-fold more potent inhibitor of H-PGDS than its corresponding nitrile **1b**, while the 8-methoxy-*N*-methylquinoline-3-carboxamide **1e** ($IC_{50} = 7,700$ nM, LE = 0.45) was equipotent with its nitrile **1c**. Structural analysis showed that a vector emanating from this 3-position points toward a channel that exits to bulk water and would be an excellent position from which to append groups on the quinoline core to enhance binding or improve drug properties. Thus, a hit-to-lead campaign strategy was undertaken to explore the 3-position of the 7-methoxyquinoline ring via array chemistry by coupling various amines to quinoline-3-carboxylic acids. The chemistry goal was to improve the potency of these fragments, while maintaining ligand efficiency.

Figure 2. Co-crystal structure of inhibitor **1a** bound to rH-PGDS with GSH.

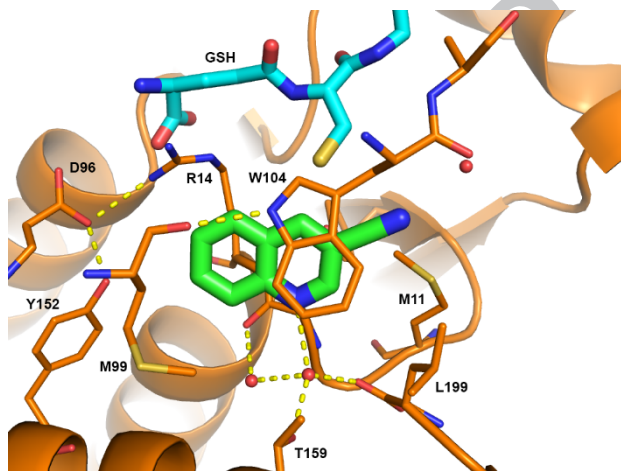


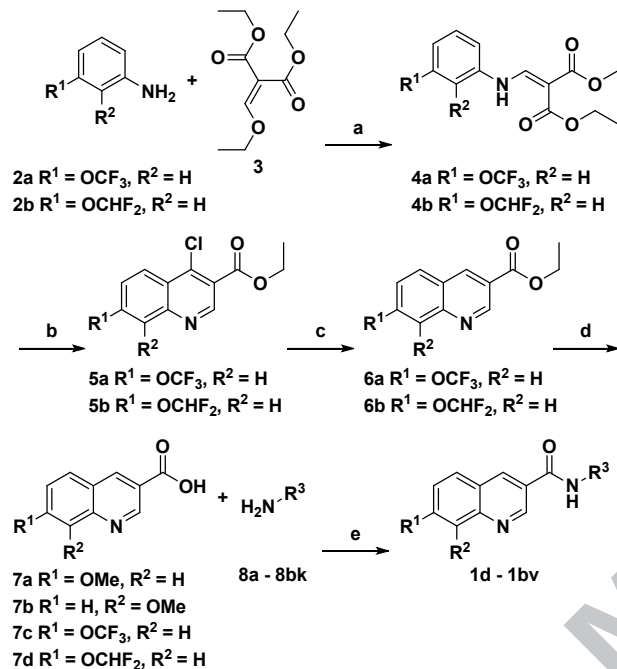
Figure 2 Legend. Ligand binding site of the X-ray co-crystal structure of **1a** complexed with rH-PGDS and GSH. The rH-PGDS carbons are colored orange with inhibitor **1a** carbons colored green and GSH carbons colored cyan. Hydrogen bonds are depicted as yellow dashed lines. The coordinates have been deposited in the Brookhaven Protein Data Bank (PDB code 6N69). This figure was generated using PyMOL version 1.7.64.6 (The PyMOL Molecular Graphics System, Version 1.7.64 Schrodinger, LLC).

1.2 Chemistry

The quinoline-3-carboxamides were prepared as depicted in Scheme 1. First, anilines **2a-2b** were thermally condensed with diethyl 2-(ethoxymethylene)malonate **3** via Michael addition and ethanol β -elimination to afford the phenylaminomethylenemalonates **4a-4b**.³³ Subsequent phosphorus oxychloride catalyzed Friedel-Craft cyclic acylation of the phenylaminomethylenemalonates **4a-4b** provided the 4-chloroquinolines **5a-5b**. Then, the 4-chloro substituents were removed via palladium-catalyzed hydrogenation to give the quinoline esters **6a-6b**.³⁴ Hydrolysis

of esters **6a-6b** with metal hydroxides afforded the 3-quinoline acids **7c-7d**. Commercially available 3-quinoline carboxylic acids **7a-7b**, as well as 3-quinoline acids **7c-7d**, were coupled with various commercially available amines **8a-8ar**, **8au-8bd**, and **8bh-8bk** or amines **8as-8at** and **8be-8bg**, known in the chemical literature, to provide the desired 3-quinoline carboxamides **1d-1bv**.

Scheme 1. Synthesis of 3-quinoline carboxamides **1d-1bv**.



Reagents and conditions: a) PhMe, 120 °C or EtOH, 65 °C, 99%; b) POCl₃, sealed tube, 125-150 °C, 31-33%; c) Pd(PPh₃)₂Cl₂, Et₃SiH, MeCN, 80 °C or H₂/Pd-C, EtOH, 93-96%; d) LiOH or NaOH, THF or MeOH, H₂O, 50 °C, 56-96%; e) T3P® or HATU, iPr₂NEt, CH₂Cl₂ or THF or DMF, 7-95%.

1.3 Results and discussion

Exploration of the 3-position began with simple aliphatic amines. The primary carboxamide **1f** (IC₅₀ = 8,900 nM) was a slightly less active inhibitor of H-PGDS than its N-methyl congener **1d**, while the tertiary dimethylcarboxamide **1g** (IC₅₀ = >50,000 nM) had no measurable inhibitory activity. Subsequent co-crystal structures revealed that the carboxamide NH forms a hydrogen bond with the cysteine sulfur of the glutathione cofactor (*vide infra*). Loss of this intramolecular interaction and occupation of the glutathione cofactor binding pocket likely accounts for this large loss of inhibitory activity. Both the ethyl and isopropyl carboxamides **1h** (IC₅₀ = 1,600 nM) and **1i** (IC₅₀ = 870 nM) are more potent than the methyl congener **1d**, while the *tert*-butyl carboxamide **1j** (IC₅₀ = 2,400 nM) has similar potency. Thus, analysis of the initial structure activity relationships from the amide coupling array chemistry revealed that disubstitution at the α-carbon of the amine enhanced potency and a free NH moiety was crucial for inhibition.

Since the isopropyl carboxamide **1i** had submicromolar inhibitory activity, a series of heteroaryl carboxamides were prepared, following Scheme 1, with the goals of establishing additional π-stacking interactions and/or hydrogen bonds with the protein or glutathione cofactor and potentially enhancing water solubility relative to the hydrophobic alkyl derivatives. All of the synthesized heteroaryl analogs enhanced inhibitory activity, with the thiazole **1k** (IC₅₀ = 49 nM) and pyrazoles **1o** (IC₅₀ = 57 nM) and **1n** (IC₅₀ = 200 nM) being more active than the imidazole **1l** (IC₅₀ = 390 nM). The differences in activity of these analogs likely result from the energetic differences of their relative desolvation. Furthermore, substitution adjacent to the amine functionality was detrimental to H-PGDS potency (compare **1m** (IC₅₀ = 8,500 nM) to **1l** or **1q** (IC₅₀ = 220 nM) to **1o**), while more distal substitution was tolerated (compare **1p** (IC₅₀ = 78 nM) and **1r** (IC₅₀ = 73 nM) to **1o**), with larger groups leading to more potent analogs (compare **1s** (IC₅₀ = 23 nM) and **1t** (IC₅₀ = 17 nM) to **1o**), albeit with decreases in ligand efficiency.

Heteroaryl rings extended from the amino group by a single atom linker were also synthesized following Scheme 1 to further explore potential protein/cofactor binding interactions. Although the benzyl derivative **1u** ($IC_{50} = 71$ nM) exhibited similar activity to the shorter thiazole **1k**, all compounds with increased hydrophilic heteroaryl analogs, including the pyrazoles **1v** ($IC_{50} = 320$ nM), **1w** ($IC_{50} = 160$ nM), and **1x** ($IC_{50} = 360$ nM), imidazole **1y** ($IC_{50} = 530$ nM), triazole **1z** ($IC_{50} = 4,500$ nM), tetrazole **1aa** ($IC_{50} = 420$ nM), pyrazines **1ab** ($IC_{50} = 1,400$ nM) and **1ae** ($IC_{50} = 2,300$ nM), pyrimidines **1ac** ($IC_{50} = 1,400$ nM), **1ad** ($IC_{50} = 1,400$ nM), and **1af** ($IC_{50} = 2,000$ nM), and 2-pyridone **1ag** ($IC_{50} = 250$ nM) were less potent H-PGDS inhibitors than the thiazole **1k**. Furthermore, ring substituents (compare **1v** to **1w** and **1x**) and methylene linker substituents (compare **1ab** to **1ae** and **1ac** to **1af**) in this benzylic series provided no increased inhibitory activity.

As shown in Table 1, the saturated cyclopentyl and cyclohexyl analogs **1ah** ($IC_{50} = 200$ nM) and **1ai** ($IC_{50} = 100$ nM) were more potent inhibitors than the corresponding isopropyl derivative **1i**. Saturated rings with their sp^3 character can disrupt crystal packing density, potentially enhancing dissolution. To explore this concept, an array of aliphatic analogs with potential hydrogen bond donor/acceptor moieties were prepared, hoping to maintain and/or improve inhibitory activity while enhancing solubility. Many of the saturated ring analogs, such as the tetrahydropyran **1aj** ($IC_{50} = 170$ nM), the cyclohexanol **1ak** ($IC_{50} = 110$ nM), the piperidine amide **1al** ($IC_{50} = 250$ nM), the piperidine sulfonamide **1am** ($IC_{50} = 110$ nM), and the δ -lactam **1an** ($IC_{50} = 220$ nM), exhibited similar potencies to their saturated counterparts **1ah** and **1ai**. Potency was maintained, despite higher desolvation energies for these compounds and indicated that an additional protein interaction might be established that compensates for the desolvation cost. In contrast, the less constrained analogs, such as the ethyleneurea **1ao** ($IC_{50} = 520$ nM), the glycineamide **1ap** ($IC_{50} = 6,900$ nM), and the alaninamides **1aq** ($IC_{50} = 1,800$ nM) and **1ar** ($IC_{50} = 7,800$ nM), were poor inhibitors of the enzyme.

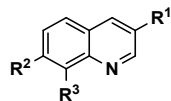
As a follow up to these results, the tetrahydrofuran **1as** ($IC_{50} = 590$ nM) was prepared and it was found to be slightly less active than the tetrahydropyran **1aj**. In contrast, the γ -lactam had similar potency to the δ -lactam **1an**, with most of the activity residing in the (*S*)-enantiomer **1at** ($IC_{50} = 98$ nM), rather than the (*R*)-isomer **1au** ($IC_{50} = 15,000$ nM). Substituted lactams, such as the *N*-methyl analog **1av** ($IC_{50} = 1,400$ nM), the 4-hydroxy analog **1ax** ($IC_{50} = 640$ nM), and the 3-methyl analog **1ay** ($IC_{50} = 4,100$ nM), as well as the isoxazolidine **1aw** ($IC_{50} = 630$ nM) and the indoline **1az** ($IC_{50} = 350$ nM), had less inhibitory activity. In contrast, the more lipophilic indene **1ba** ($IC_{50} = 16$ nM) was 20-fold more potent than the indoline **1az**, likely because of a reduced energetic desolvation penalty upon binding to the enzyme. The location of the lactam carbonyl was important for maximum inhibition as the isomeric γ -lactams **1bb** ($IC_{50} = 1,200$ nM) and **1bc** ($IC_{50} = 620$ nM) were less active than **1at**.

The unsubstituted piperidine **1bd** ($IC_{50} = 2,200$ nM) was 20-fold less potent than the piperidine sulfonamide **1am**. The decrease in inhibitory potency may be the result of either the overt positive charge and/or the significantly higher desolvation cost on binding. Despite having a high polar surface area with accompanying high desolvation, the piperidine tetrazole **1be** ($IC_{50} = 56$ nM) is 4-fold more potent than the piperidine amide **1al**. Furthermore, the piperidine thiazole **1bf** ($IC_{50} = 9.7$ nM) is an even better H-PGDS inhibitor than **1be**. The lower polar surface (67 \AA^2 versus 98 \AA^2) likely explains this increase in inhibition.

Other cyclohexyl derivatives, prepared to follow up on the cyclohexanol analog **1ak**, also exhibited good H-PGDS inhibitory activity, with the tertiary alcohols **1bg** ($IC_{50} = 25$ nM) and **1bk** ($IC_{50} = 26$ nM), as well as the amide **1bh** ($IC_{50} = 57$ nM), being slightly more potent than the tertiary alcohol **1bi** ($IC_{50} = 120$ nM). Furthermore, the spiro[3.3]heptane cyclohexyl mimic **1bj** ($IC_{50} = 8.2$ nM) is an even more potent inhibitor than **1bg**. Interestingly, the amine analog **1bl** ($IC_{50} = 14$ nM), in which the basicity of the amine has been attenuated via the electron withdrawing ability of the 2,2,2-trifluoroethyl group, also exhibits excellent inhibitory activity, as compared to the more basic piperidine analog **1bd**.

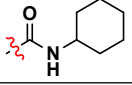
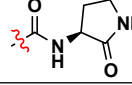
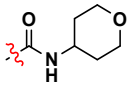
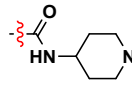
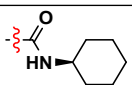
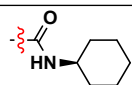
Since the spiro[3.3]heptane analog **1bj** was an extremely potent inhibitor, several four-membered ring analogs were prepared with the aim of reducing the molecular weight and lipophilicity, while improving water solubility and maintaining potency. These analogs were less active inhibitors than the parent cyclohexanol **1ak**, with the *cis* alcohols **1bm** ($IC_{50} = 340$ nM) and **1bo** ($IC_{50} = 280$ nM) being more active than the *trans* congeners **1bn** ($IC_{50} = 500$ nM) and **1bp** ($IC_{50} = 610$ nM).

Table 1. H-PGDS enzyme inhibition data.



#	R^1	R^2	R^3	$IC_{50} \pm S.D.^a$ nM	#	R^1	R^2	R^3	$IC_{50} \pm S.D.^a$ nM
1a	CN	H	H	>50000	1al		OCH ₃	H	250 ±110
1b	CN	OCH ₃	H	13000 ±7800	1am		OCH ₃	H	110 ±43
1c	CN	H	OCH ₃	8400 ±3100	1an		OCH ₃	H	220 ±110
1d		OCH ₃	H	3100 ±1700	1ao		OCH ₃	H	520 ±220
1e		H	OCH ₃	7700 ±2500	1ap		OCH ₃	H	6900 ±8700
1f		OCH ₃	H	8900 ±2300	1aq		OCH ₃	H	1800 ±960
1g		OCH ₃	H	>50000	1ar		OCH ₃	H	7800 ±2400
1h		OCH ₃	H	1600 ±240	1as		OCH ₃	H	590 ±160
1i		OCH ₃	H	870 ±350	1at		OCH ₃	H	98 ±42
1j		OCH ₃	H	2400 ±480	1au		OCH ₃	H	15000 ±8800
1k		OCH ₃	H	49 ±37	1av		OCH ₃	H	1400 ±1100
1l		OCH ₃	H	390 ^b ±25	1aw		OCH ₃	H	630 ±85
1m		OCH ₃	H	8500 ^c ±5500	1ax		OCH ₃	H	640 ±310
1n		OCH ₃	H	200 ±39	1ay		OCH ₃	H	4100 ±2300
1o		OCH ₃	H	57 ±27	1az		OCH ₃	H	350 ±110
1p		OCH ₃	H	78 ±35	1ba		OCH ₃	H	16 ±6.5

1q		OCH ₃	H	220 ±58	1bb		OCH ₃	H	1200 ±740
1r		OCH ₃	H	73 ±11	1bc		OCH ₃	H	620 ±290
1s		OCH ₃	H	23 ±12	1bd		OCH ₃	H	2200 ±480
1t		OCH ₃	H	17 ±5	1be		OCH ₃	H	56 ±64
1u		OCH ₃	H	71 ±54	1bf		OCH ₃	H	9.7 ±3.9
1v		OCH ₃	H	320 ±280	1bg		OCH ₃	H	25 ±3.4
1w		OCH ₃	H	160 ±130	1bh		OCH ₃	H	57 ±23
1x		OCH ₃	H	360 ±320	1bi		OCH ₃	H	120 ±12
1y		OCH ₃	H	530 ±140	1bj		OCH ₃	H	8.2 ±2.4
1z		OCH ₃	H	4500 ±3300	1bk		OCH ₃	H	26 ±5.3
1aa		OCH ₃	H	420 ±210	1bl		OCH ₃	H	14 ±2.2
1ab		OCH ₃	H	1400 ±920	1bm		OCH ₃	H	340 ±190
1ac		OCH ₃	H	1400 ±760	1bn		OCH ₃	H	500 ±230
1ad		OCH ₃	H	1400 ±710	1bo		OCH ₃	H	280 ±27
1ae		OCH ₃	H	2300 ±1100	1bp		OCH ₃	H	610 ±98
1af		OCH ₃	H	2000 ±900	1bq		OCF ₃	H	230 ±48
1ag		OCH ₃	H	250 ±230	1br		OCF ₃	H	120 ±28
1ah		OCH ₃	H	200 ±92	1bs		OCF ₃	H	15 ±5.2

1ai		OCH ₃	H	100 ±61	1bt		OCHF ₂	H	52 ±13
1aj		OCH ₃	H	170 ±81	1bu		OCHF ₂	H	20 ±6.8
1ak		OCH ₃	H	110 ±44	1bv		OCHF ₂	H	9.9 ±2.7

^aS.D. = standard deviation; mean ± S.D. All inhibitors were tested with N ≥ 4 unless otherwise noted.

^bN = 2.

^cN = 3.

Many of these compounds had H-PGDS inhibitory potencies less than 100 nM in the enzymatic assay. Some also had reduced plasma protein binding with free fractions of greater than 5%, resulting in small potency decreases in a rat basophilic leukemia (RBL) cell PGD₂ production assay relative to the H-PGDS enzymatic assay. Despite their good *ex vivo* H-PGDS inhibitory potency, these analogs all contained a 3-carboxamide moiety. Carboxamides are susceptible to hydrolysis by amidases *in vivo* and some of these analogs were enzymatically degraded to the corresponding carboxylic acid in a whole blood assay (e.g. human whole blood assay % remaining after 1 hour: **1j** = 1%, **1n** = 63%). Substitution was the key to amidase recognition with certain substituents presumably being poor substrates of the putative amidase and having increased plasma stability (e.g. human whole blood assay % remaining after 1 hour: **1o** = 93%, **1at** = 100%).

These analogs also all contained a 7-methoxyquinoline moiety. These 7-methoxyquinoline-3-carboxamides are quite electron rich, very UV active, and could exhibit phototoxicity. In fact, some of the analogs degrade over time when exposed to UV light. Furthermore, aryl methoxy groups are a potential metabolic liability due to their potential for oxidative *O*-dealkylation of the methyl moiety to produce quinolin-7-ols. The phenolic metabolites may have reduced H-PGDS inhibitory activity and are susceptible to secondary phase metabolism with the resulting conjugates having increased renal clearances. Therefore, the stability of a representative analog **1bg** was studied in a mouse liver microsome assay and it exhibited at short *in vitro* half-life ($t_{1/2}$ = 38 minutes).

Hypothesizing that this metabolic instability arose from *O*-methyl dealkylation, analogs of **1at**, **1be**, and **1bg** were prepared that replaced the methyl moiety with more electron deficient difluoromethyl or trifluoromethyl in attempts to increase the metabolic stability of these H-PGDS inhibitors. These electron withdrawing substitutions also attenuate the UV absorbance of these isomers, enhancing their photostability. The trifluoromethyl derivatives **1bq** (IC₅₀ = 230 nM), **1br** (IC₅₀ = 120 nM), and **1bs** (IC₅₀ = 15 nM) tended to be less potent inhibitors of H-PGDS than their difluoromethyl analogs **1bt** (IC₅₀ = 52 nM), **1bu** (IC₅₀ = 20 nM), and **1bv** (IC₅₀ = 9.9 nM). The best two of these competitive, reversible, potent analogs, **1bs** (RBL IC₅₀ = 100 nM) and **1bv** (RBL IC₅₀ = 100 nM), also exhibited good cellular activity in the rat basophilic leukemia (RBL) cell PGD₂ production assay and were substantially more stable in mouse liver microsomes, both having *in vitro* half-lives of greater than 180 minutes, supporting the *O*-demethylation hypothesis.

Furthermore, as shown in Table 2, both **1bs** (P_{APP} = 470 nm/sec) and **1bv** (P_{APP} = 240 nm/sec) were highly permeable in an artificial membrane permeability assay that served as a surrogate for the more labor intensive Madin-Darby canine kidney (MDCK) cell permeation assay.³⁵ Thus, the oral bioavailability of these analogs should not be limited by absorption across cell membranes. Additionally, the fasted state simulated intestinal fluid solubility's of **1bs** (FaS-SIF = 0.016 mg/mL) and **1bv** (FaS-SIF = 0.070 mg/mL) were modest, but due to their high permeability, acceptable for *i.v.* and *p.o.* pharmacokinetic profiling.³⁶

With the view of identifying a suitable tool compound to explore the pharmacodynamics of H-PGDS inhibitors in murine models of inflammatory diseases, the pharmacokinetic parameters of these compounds were determined in mice. The trifluoromethyl analog **1bs** had a low *i.v.* clearance (C₁ = 3.8 mL/min/kg), moderate steady state volume of distribution (V_{SS} = 2.5 L/kg), and long terminal half-life ($t_{1/2}$ = 7.9 h). The compound also exhibited good oral exposure (*p.o.* DNAUC = 1900 ng/hr/mL) with a moderate oral bioavailability (F = 46%). The difluoromethyl

analog **1bv** also had a low *i.v.* clearance ($C_1 = 5.6$ mL/min/kg), moderate steady state volume of distribution ($V_{SS} = 1.7$ L/kg), and long terminal half-life ($t_{1/2} = 3.8$ h), as well as good oral exposure (*p.o.* DNAUC = 1800 ng/hr/mL) with a higher oral bioavailability ($F = 61\%$).

Table 2. H-PGDS inhibitor pharmacokinetic data

#	P_{APP}	FaS-SIF	Microsomes	$t_{1/2}$	C_1	V_{SS}	F	DNAUC
	nm/sec	mg/mL	$t_{1/2}$ min	h	mL/min/kg	L/kg	%	ng/hr/mL
1bs	470	0.016	>180	7.9	3.8	2.5	46	1900
1bv	240	0.070	>180	3.8	5.6	1.7	61	1800

To further explore the suitability of compound **1bv** for *in vivo* studies, its binding kinetics were determined. The dissociation constant K_d for **1bv** ($K_d = 0.50 \pm 0.08$ nM) was measured in the presence of glutathione (1 mM) by equilibrium titration of the quenching of the indole intrinsic fluorescence of ^{104}Trp in the active site with **1bv** excited at 285 nm. The k_{on} of **1bv** ($k_{on} = 5.4 \pm 0.19 \times 10^6$ M⁻¹sec⁻¹) was measured by stopped-flow spectrofluorimetry from the fastest phase of intrinsic tryptophan quench time courses, while the k_{off} (calculated $k_{off} = 0.0027$ sec⁻¹) was calculated from the values of K_d and k_{on} ($K_d = k_{off}/k_{on}$). Inhibitor **1bv** rapidly associates with and dissociates from H-PGDS. This K_d is a better reflection of the intrinsic potency of **1bv** as compared to the IC_{50} of **1bv**, which is elevated due to prostaglandin substrate competition and active site titration of hH-PGDS in the activity assay.

Several other enzymes also employ PGH_2 as a substrate to produce prostanoids. Their inhibition by an H-PGDS inhibitor tool compound could confound the interpretation of pharmacodynamic studies in inflammatory models of disease, therefore the selectivity of inhibitor **1bv** versus two closely related synthase enzymes in the prostanoid pathway was also determined. Analog **1bv** was tested against lipocalin prostaglandin D synthase (L-PGDS, *vide supra*)¹⁵ and microsomal prostaglandin E synthase (m-PGES)³⁷ and did not inhibit either enzyme at concentrations up to 30,000 nM, supporting its suitability for use *in vivo* to probe the effects of H-PGDS inhibition.

Furthermore, the general off-target liabilities of **1bv** were also evaluated. Compound **1bv** did not block the human ether-a-go-go-related gene potassium ion channel ($K_v11.1$)³⁸ or inhibit cytochrome p450 3A4 monooxygenase enzyme at concentrations up to 30,000 nM. Also, at concentrations up to 10,000 nM, **1bv** did not inhibit a broad panel of proteins, including 7-TM receptors (5HT_{1B}, 5HT_{2A}, 5HT_{2C}, α_{2C} , β_2 , κ , μ , A_{2A}, CB₂, D₁, D₂, H₁, M₁, M₂, NK₁, V_{1A}), ion channels (5HT₃, Ca_v1.2, GABA_A, K_v7.1, Na_v1.5, NMDA), enzymes (AChE, COX-2, MAO-B, PDE_{3A}, PDE_{4B}), transcription factors (AhR, AR, PXR), kinases (Aurora B, LCK, PI3K γ), and transporters (NET, OATP_{1B1}, SERT). Coupled with its high H-PGDS inhibitory potency and good pharmacokinetic characteristics, this profile makes **1bv** a suitable tool compound for studying the pharmacodynamic effects of H-PGDS inhibition.

Inhibitor **1bv** was profiled in a murine mast cell degranulation model of inflammation to evaluate the acute effects of a H-PGDS inhibitor on mast cell release of PGD_2 .³⁹ Male C57BL/6J mice were administered *p.o.* with vehicle or H-PGDS inhibitor **1bv** at various doses (0.03, 0.1, 0.3, 1, 3 mg/kg), then anesthetized and challenged one hour later with vehicle (PBS) or the *N*-methyl-*p*-methoxyphenethylamine/formaldehyde synthetic polymer 48/80 (i.p. 0.75 mg/mL) with abdomen massage. After seven minutes, blood was collected (**1bv** analysis), the mice were euthanized, and lavage fluid was collected from the abdominal cavity (PGD_2 analysis). As shown in Figure 3, the mast cell secretagogue 48/80 induces production and release of PGD_2 into peritoneal lavage fluid versus phosphate buffered saline (PBS). H-PGDS inhibitor **1bv** attenuates this PGD_2 release to baseline levels in a dose-dependent manner with an $ED_{50} = 0.032$ mg/kg (**1bv** blood $EC_{50} = 21$ nM) in this acute inflammation model. Levels of the related prostaglandin PGE_2 were not significantly different between **1bv** treated and untreated animals after challenge with synthetic polymer 48/80.

Figure 3. H-PGDS inhibition blocks 48/80 challenge-induced PGD_2 production *in vivo*

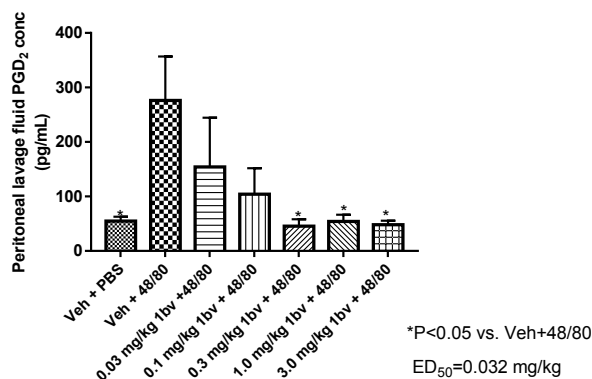


Figure 3 Legend: Young adult male C57BL/6J mice were administered (p.o.) vehicle or the H-PGDS inhibitor **1bv** at varying doses (from 0.03 mg/kg to 3 mg/kg). One hour later, mice were anesthetized, injected with (i.p.) 0.2 mL vehicle or 48/80 (0.75 mg/mL), and peritoneal lavage fluid was collected after 7 minutes. (A) Data are presented as means ($n = 7/\text{group}$) \pm S.E.M. and analyzed using ANOVA followed by Dunnett's comparing vehicle+48/80 to respective treatment group.

To gain further understanding of the binding mode of quinoline H-PGDS inhibitors, a protein co-crystal structure of inhibitor **1bv** bound with hH-PGDS and GSH was obtained. As shown in Figure 4, the bound structure of **1bv** has many similarities to that of fragment **1a**. Both utilize the quinoline nitrogen to form a key hydrogen bond with a tightly bound water molecule (structural water oxygen to quinoline nitrogen distance = 2.8 Å) coordinated by ¹⁹⁹Leu, ¹⁵⁹Thr, and an additional water molecule (vide supra). Both compounds also form a face to face π - π stacking interaction between the quinoline ring and the indole side chain of ¹⁰⁴Trp (face of indole ¹⁰⁴Trp to face of quinoline **1bv** distance = 3.6 Å). In addition, the quinoline 3-carboxamide NH forms a hydrogen bond with the sulfur of the glutathione cofactor cysteine residue. This interaction likely accounts for the 4-fold gain in potency between the nitrile **1b** and the N-methyl carboxamide **1d**. Also, the difluoromethoxy group extends into a small hydrophobic pocket formed by ⁹⁹Met, ¹⁵⁵Ile, and ¹³Gly. Additionally, the electron releasing character of the difluoromethoxy group leads to increased basicity of the quinoline nitrogen that results in an enhanced polar interaction between that nitrogen and the coordinating water molecule. The combination of enhanced polar and hydrophobic contacts could explain the 10-fold increase in inhibitory activity of **1b** versus the starting fragment **1a**. Finally, the chair conformation of the cyclohexyl moiety enhances binding through hydrophobic interactions with the side chains of ¹⁰⁵Ala and ⁹Phe. These interactions help explain the ~500-fold gain in activity of **1bg** versus **1d**. The tertiary alcohol is mostly solvent exposed, adding little to ligand binding, but enhancing water solubility of this analog. Thus, these human H-PGDS co-crystal structures bound with ligand and cofactor not only provide structural insight into the binding requirements of the enzyme, but also help to rationalize much of the SAR observed in the quinoline carboxamide inhibitor series.

Figure 4. Co-crystal structure of inhibitor **1bv** bound to hH-PGDS with GSH.

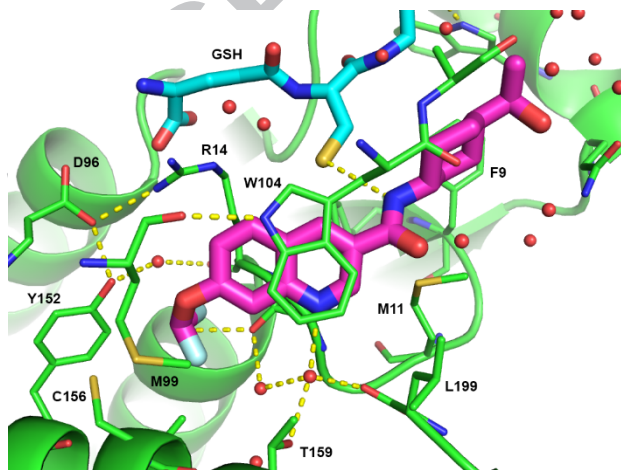


Figure 4 Legend. Ligand binding site of the X-ray co-crystal structure of **1bv** complexed with hH-PGDS and glutathione (GSH). The hH-PGDS carbons are colored green with inhibitor **1bv** carbons colored magenta and GSH carbons colored cyan. Hydrogen bonds are depicted as yellow dashed lines. The coordinates have been deposited in the Brookhaven Protein Data Bank (PDB code 6N4E). This figure was generated using PyMOL version 1.7.64.6 (The PyMOL Molecular Graphics System, Version 1.7.64 Schrodinger, LLC).

1.4 Conclusion

In this work, further evidence of the utility of fragment-based drug discovery to deliver optimizable chemical matter for robust lead development is provided. A diverse set of confirmed hits, derived from ligand-bound protein crystal structures of H-PGDS, were clustered by binding mode and resulted in the identification of a cluster containing the 6,6-fused heterocyclic quinoline **1a**. Through SAR by catalog, array chemistry, traditional medicinal chemistry, and structure-based design, this initial hit was developed into a H-PGDS chemical tool compound, GSK2894631A **1bv**, with excellent potency, selectivity, and similar ligand efficiency (LE = 0.42) to the starting fragment **1a**. Furthermore, **1bv** exhibited good pharmacokinetic parameters in mice and dose-dependently attenuated PGD₂ production and secretion in a mast cell degranulation assay pharmacodynamic model of inflammation. Further publications from these laboratories will explore its use in other prostaglandin-driven inflammation models.

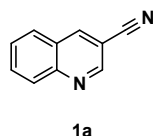
1.5 Experimental section

All commercial chemicals and solvents were reagent grade and were used without further purification unless otherwise specified. The following abbreviations are utilized in the manuscript: tetrahydrofuran (THF), diethyl ether (Et₂O), dimethyl sulfoxide (DMSO), ethyl acetate (EtOAc), dichloromethane (CH₂Cl₂), trifluoroacetic acid (TFA), N,N-dimethylformamide (DMF), methanol (MeOH), dimethoxyethane (DME), N-methylpyrrolidine (NMP), acetonitrile (MeCN), chloroform (CHCl₃), phosphorus oxychloride (POCl₃), magnesium sulfate (MgSO₄), triethylamine (Et₃N), 2-propanol (iPrOH), diisopropylethylamine (iPr₂NEt), sodium hydroxide (NaOH), t-butylmethyl ether (TBME), acetic acid (AcOH or HOAc), ethanol (EtOH), di-tert-butylidicarbonate (BOC₂O), sodium sulfate (Na₂SO₄), N,N-dimethylacetamide (DMA), sodium bicarbonate (NaHCO₃), potassium carbonate (K₂CO₃), 1-[bis(dimethylamino)methylene]-1H-1,2,3-triazolo[4,5-b]pyridinium 3-oxid hexafluorophosphate (HATU), azobis(isobutyronitrile) (AIBN), 4-(2-hydroxyethyl)-piperazine-1-ethanesulfonic acid (HEPES), and dithiothreitol (DTT). All reactions except those in aqueous media were carried out with the use of standard techniques for the exclusion of moisture. Reactions were monitored by thin-layer chromatography (TLC) on 0.25 mm silica gel plates (60F-254, E. Merck) and visualized with UV light, iodine, iodoplatinate, potassium permanganate, cerium molybdate, or 5% phosphomolybdic acid in 95% ethanol. Final compounds were typically purified either by flash chromatography on silica gel (E. Merck 40–63 mm), radial chromatography on a Chromatotron™ using prepared silica gel plates, or on a Biotage Horizon or ISCO Combiflash® pump and fraction collection system utilizing prepacked silica gel. Analytical purity was assessed either by reversed-phase high performance liquid chromatography (RP-HPLC) using an Agilent 1100 system equipped with a diode array spectrometer (λ range 190–400 nm) or by the LC-MS method detailed below. The stationary phase was a Keystone Scientific BDS Hypersil™ C-18 column (5 μm, 4.6 mm × 200 mm). The mobile phase employed 0.1% aqueous TFA with MeCN as the organic modifier and a flow rate of 1.0 mL/min. Analytical data are reported as retention time (t_R) in minutes and percent purity. All compounds were found to be ≥95% pure unless otherwise indicated. ¹H NMR spectra were recorded on either a Varian Unityplus™ 400 MHz or a Bruker Avance™ III 400 MHz NMR spectrometer. Chemical shifts are reported in parts per million (ppm, δ units). Coupling constants are reported in units of hertz (Hz). Splitting patterns are designated as s, singlet; d, doublet; t, triplet; q, quartet; p, pentet; h, hextet; m, multiplet; or br, broad. Low-resolution mass spectra (MS) were recorded on a Waters SQD. High-resolution MS were recorded on a Waters (Micromass®) LCT time-of-flight mass spectrometer. Low-resolution mass spectra were obtained under electrospray ionization (ESI), atmospheric pressure chemical ionization (APCI), or fast atom bombardment (FAB) methods. All studies were conducted in accordance with the GSK Policy on the Care, Welfare and Treatment of Laboratory Animals and were reviewed the Institutional Animal Care and Use Committee either at GSK or by the ethical review process at the institution where the work was performed.

General amide bond coupling method A. N,N-Diisopropylethylamine (4.0 eq) was added to acid (1 eq) in solvent (dichloromethane, tetrahydrofuran, or N,N-dimethylformamide, 0.05 to 0.2 M) at room temperature. Then, amine (1.0-2.0 eq) was added and the reaction mixture was stirred for five minutes. Then, n-propylphosphonic acid anhydride (2.0 eq) was added and the reaction mixture was stirred for sixteen hours. The reaction mixture was concentrated. The resulting residue was purified by RP HPLC or silica gel chromatography to give the quinoline-3-carboxamide (25%-86 % yield).

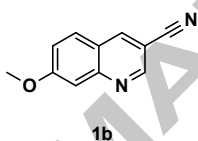
General amide bond coupling method B. *N,N*-Diisopropylethylamine (3.0–4.0 eq) was added to 8-methoxyquinoline-3-carboxylic acid (1.0 eq) in solvent (dichloromethane, tetrahydrofuran, or *N,N*-dimethylformamide, 0.05 to 0.2 M) at room temperature. Then, 1-((dimethylamino)(dimethyliminio)methyl)-1H-[1,2,3]triazolo[4,5-*b*]pyridine 3-oxide hexafluorophosphate(V) (1.0-1.5 eq) was added and the reaction mixture was stirred for five minutes. Then, amine (1.0 – 2.0 eq) was added and the reaction mixture was stirred for one to sixteen hours. 10% Aqueous citric acid was added and the reaction mixture was extracted with dichloromethane, washed with saturated sodium bicarbonate, dried over magnesium sulfate, filtered, and concentrated. The resulting residue was purified by RP HPLC or silica gel chromatography to give the quinoline-3-carboxamide (1%-95 % yield).

Quinoline-3-carbonitrile 1a.



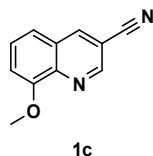
Commercial (Aldrich); ¹H NMR (400 MHz, CD₃SOCD₃) δ 9.17 (d, 1H, J = 2 Hz), 9.09 (d, 1H, J = 2 Hz), 8.13 (d, 1H, J = 8 Hz), 8.11 (d, 1H, J = 8 Hz), 7.98 (ddd, 1H, J = 8, 7, 2 Hz), 7.78 (ddd, 1H, J = 8, 7, 1 Hz); LC-MS (LC-ES) M+H = 155.

7-Methoxyquinoline-3-carbonitrile 1b.



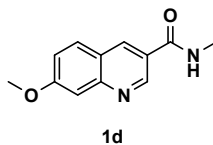
Commercial (Biofine); ¹H NMR (400 MHz, CD₃SOCD₃) δ 9.08 (d, 1H, J = 2 Hz), 8.94 (d, 1H, J = 2 Hz), 8.00 (d, 1H, J = 9 Hz), 7.48 (d, 1H, J = 2 Hz), 7.41 (dd, 1H, J = 9, 2 Hz), 3.97 (s, 3H); LC-MS (LC-ES) M+H = 185.

8-Methoxyquinoline-3-carbonitrile 1c.



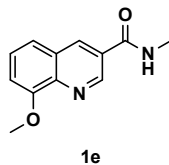
Commercial (Astatech); ¹H NMR (400 MHz, CD₃SOCD₃) δ 9.09 (d, 1H, J = 2 Hz), 9.03.76 (d, 1H, J = 2 Hz), 7.69 (t, 1H, J = 8 Hz), 7.61 (dd, 1H, J = 8, 1 Hz), 7.41 (dd, 1H, J = 8, 1 Hz), 3.99 (s, 3H); LC-MS (LC-ES) M+H = 185.

7-Methoxy-*N*-methylquinoline-3-carboxamide 1d.



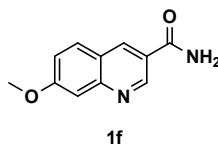
Commercial (Aurora Building Blocks); **Method B**; 7-Methoxyquinoline-3-carboxylic acid **7a** (Astatech); Methyl amine **8a** (Aldrich); *N,N*-Dimethylformamide; 46% yield; ¹H NMR (400 MHz, CDCl₃) δ 9.19 (d, 1H, J = 2 Hz), 8.60 (d, 1H, J = 2 Hz), 7.78 (d, 1H, J = 8 Hz), 7.45 (d, 1H, J = 2 Hz), 7.26 (dd, 1H, J = 8, 2 Hz), 6.76 (br s, 1H), 3.98 (s, 3H), 3.08 (d, 3H, J = 5 Hz); LC-MS (LC-ES) M+H = 217.

8-Methoxy-*N*-methylquinoline-3-carboxamide 1e.



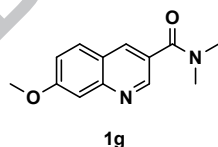
Commercial (Aurora Building Blocks); **Method A**; 8-Methoxyquinoline-3-carboxylic acid **7b** (Astatech); Methylamine **8a** (Aldrich); Dichloromethane; 86% yield; $^1\text{H NMR}$ (400 MHz, CD_3SOCD_3) δ 9.18 (d, 1H, $J = 2$ Hz), 8.80 (br q, 1H, $J = 5$ Hz), 8.72 (d, 1H, $J = 2$ Hz), 7.59 (d, 1H, $J = 5$ Hz), 7.58 (d, 1H, $J = 5$ Hz), 7.28 (t, 1H, $J = 5$ Hz), 3.97 (s, 3H), 2.84 (d, 3H, $J = 5$ Hz); LC-MS (LC-ES) $M+H = 217$.

7-Methoxyquinoline-3-carboxamide **1f**.



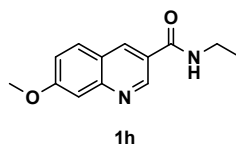
Commercial (ABC Lab); 19 M Sodium hydroxide (0.057 ml, 1.088 mmol) was added to 7-methoxyquinoline-3-carbonitrile **1b** (0.0668 g, 0.363 mmol) in dimethyl sulfoxide (1.813 ml) at room temperature, followed by 30% aqueous hydrogen peroxide (0.381 ml, 4.35 mmol) and the solution was stirred for sixty-four hours at room temperature. Water was added to the reaction mixture and it was extracted with dichloromethane (4X), dried over magnesium sulfate, filtered, and concentrated. The residue was purified by silica gel chromatography, eluting with methanol:ethyl acetate (0:1 to 2:3) to give 7-methoxyquinoline-3-carboxamide **1f** (Commercial (ABCR), 0.0352 g, 0.165 mmol, 45.6 % yield). $^1\text{H NMR}$ (400 MHz, CD_3SOCD_3) δ 9.22 (d, 1H, $J = 2$ Hz), 8.75 (d, 1H, $J = 2$ Hz), 8.22 (br s, 1H), 7.96 (d, 1H, $J = 9$ Hz), 7.59 (br s, 1H), 7.44 (d, 1H, $J = 2$ Hz), 7.31 (dd, 1H, $J = 9, 2$ Hz), 3.94 (s, 3H); LC-MS (LC-ES) $M+H = 203$.

7-Methoxy-*N,N*-dimethylquinoline-3-carboxamide **1g**.



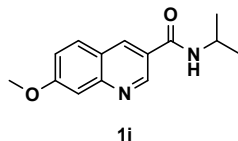
Commercial (Aurora Building Blocks); **Method A**; 7-Methoxyquinoline-3-carboxylic acid **7a** (Astatech); Dimethylamine **8b** (Aldrich); Dichloromethane; 73% yield; $^1\text{H NMR}$ (400 MHz, CD_3SOCD_3) δ 8.83 (d, 1H, $J = 2$ Hz), 8.38 (d, 1H, $J = 2$ Hz), 7.95 (d, 1H, $J = 9$ Hz), 7.42 (d, 1H, $J = 2$ Hz), 7.31 (dd, 1H, $J = 9, 2$ Hz), 3.93 (s, 3H), 3.02 (s, 6H); LC-MS (LC-ES) $M+H = 231$.

N-Ethyl-7-methoxyquinoline-3-carboxamide **1h**.



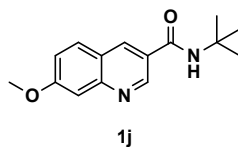
Commercial (Aurora Building Blocks); **Method A**; 7-Methoxyquinoline-3-carboxylic acid **7a** (Astatech); Ethylamine **8c** (Aldrich); Dichloromethane; 74% yield; $^1\text{H NMR}$ (400 MHz, CD_3SOCD_3) δ 9.19 (d, 1H, $J = 2$ Hz), 8.73 (br t, 1H, $J = 6$ Hz), 8.71 (d, 1H, $J = 2$ Hz), 7.98 (d, 1H, $J = 9$ Hz), 7.44 (d, 1H, $J = 2$ Hz), 7.31 (dd, 1H, $J = 9, 2$ Hz), 3.94 (s, 3H), 3.34 (dq, 2H, $J = 7, 6$ Hz), 1.16 (t, 3H, $J = 7$ Hz); LC-MS (LC-ES) $M+H = 231$.

N-(1-Methylethyl)-7-(methoxy)-3-quinolinecarboxamide **1i**.



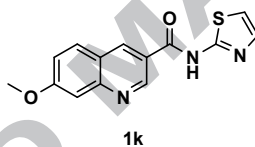
Commercial (Aurora Building Blocks); **Method B**; 7-Methoxyquinoline-3-carboxylic acid **7a** (Astatech); Isopropylamine **8d** (Aldrich); *N,N*-Dimethylformamide; 42% yield; $^1\text{H NMR}$ (400 MHz, CDCl_3) δ 9.18 (d, 1H, $J = 2$ Hz), 8.62 (d, 1H, $J = 2$ Hz), 8.24 (br s, 1H), 7.80 (d, 1H, $J = 8$ Hz), 7.51 (d, 1H, $J = 2$ Hz), 7.27 (dd, 1H, $J = 8, 2$ Hz), 4.36 (h, 1H, $J = 6$ Hz), 3.98 (s, 3H), 1.32 (d, 6H, $J = 6$ Hz); LC-MS (LC-ES) $M+H = 217$.

***N*-(tert-Butyl)-7-methoxyquinoline-3-carboxamide 1j.**



Commercial (Aurora Building Blocks); **Method B**; 7-Methoxyquinoline-3-carboxylic acid **7a** (Astatech); tert-Butylamine **8e** (Aldrich); *N,N*-Dimethylformamide; 47% yield; $^1\text{H NMR}$ (400 MHz, CD_3SOCD_3) δ 9.15 (d, 1H, $J = 2$ Hz), 8.68 (d, 1H, $J = 2$ Hz), 8.08 (d, 1H, $J = 9$ Hz), 8.03 (br s, 1H), 7.97 (d, 1H, $J = 2$ Hz), 7.31 (dd, 1H, $J = 9, 2$ Hz), 3.95 (s, 3H), 1.43 (s, 9H); LC-MS (LC-ES) $M+H = 259$.

7-(Methoxy)-*N*-1,3-thiazol-2-yl-3-quinolinecarboxamide 1k.



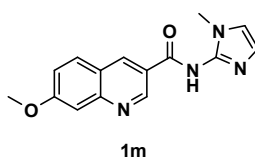
Method B; 7-Methoxyquinoline-3-carboxylic acid **7a** (Astatech); 2-Aminothiazole **8f** (Aldrich); *N,N*-Dimethylformamide; 95% yield; $^1\text{H NMR}$ (400 MHz, CDCl_3) δ 9.50 (d, 1H, $J = 2$ Hz), 8.87 (d, 1H, $J = 2$ Hz), 8.21 (s, 1H), 7.88 (d, 1H, $J = 9$ Hz), 7.52 (d, 1H, $J = 2$ Hz), 7.45 (d, 1H, $J = 3$ Hz), 7.32 (dd, 1H, $J = 9, 2$ Hz), 7.06 (d, 1H, $J = 3$ Hz), 4.02 (s, 3H); LC-MS (LC-ES) $M+H = 286$.

***N*-(1*H*-Imidazol-2-yl)-7-methoxyquinoline-3-carboxamide 1l.**



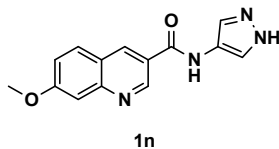
Method B; 7-Methoxyquinoline-3-carboxylic acid **7a** (Astatech); 1*H*-Imidazol-2-amine **8g** (Oakwood); *N,N*-Dimethylformamide; 81% yield; $^1\text{H NMR}$ (400 MHz, CD_3SOCD_3) δ 9.40 (s, 1H), 8.90 (s, 1H), 8.83 (d, 1H, $J = 2$ Hz), 8.39 (d, 1H, $J = 2$ Hz), 8.01 (d, 1H, $J = 9$ Hz), 7.45 (d, 1H, $J = 2$ Hz), 7.32 (dt, 1H, $J = 9, 2$ Hz), 6.86 (s, 2H), 3.95 (s, 3H); LC-MS (LC-ES) $M+H = 269$.

7-Methoxy-*N*-(1-methyl-1*H*-imidazol-2-yl)quinoline-3-carboxamide 1m.



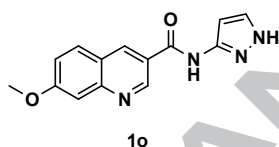
Method B; 7-Methoxyquinoline-3-carboxylic acid **7a** (Astatech); 1-Methyl-1*H*-imidazol-2-amine **8h** (Oakwood); *N,N*-Dimethylformamide; 12% yield; ¹H NMR (400 MHz, CD₃SOCD₃) δ 9.54 (br s, 1H), 8.90 (s, 1H), 8.02 (d, 1H, *J* = 9 Hz), 7.44 (d, 1H, *J* = 2 Hz), 7.28 (dd, 1H, *J* = 9, 2 Hz), 7.06 (s, 1H), 6.87 (s, 1H), 3.94 (s, 3H), 3.60 (s, 3H); LC-MS (LC-ES) M+H = 283.

7-Methoxy-*N*-(1*H*-pyrazol-4-yl)quinoline-3-carboxamide 1n.



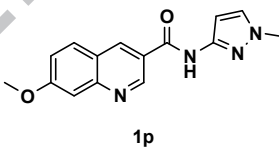
Method B; 7-Methoxyquinoline-3-carboxylic acid **7a** (Astatech); 1*H*-Pyrazol-4-ylamine **8i** (Oakwood); *N,N*-Dimethylformamide; 79% yield; ¹H NMR (600 MHz, CD₃SOCD₃) δ 12.67 (br s, 1H), 10.67 (s, 1H), 9.31 (d, 1H, *J* = 2 Hz), 8.83 (d, 1H, *J* = 2 Hz), 8.02 (d, 1H, *J* = 9 Hz), 7.89 (br s, 2H), 7.48 (d, 1H, *J* = 3 Hz), 7.35 (dd, 1H, *J* = 9, 3 Hz), 3.96 (s, 3H); LC-MS (LC-ES) M+H = 269.

7-Methoxy-*N*-(1*H*-pyrazol-3-yl)quinoline-3-carboxamide 1o.



Method B; 7-Methoxyquinoline-3-carboxylic acid **7a** (Astatech); 3-Aminopyrazole **8j** (Oakwood); *N,N*-Dimethylformamide; 12% yield; ¹H NMR (600 MHz, CD₃SOCD₃) δ 12.51 (br s, 1H), 11.11 (br s, 1H), 9.31 (d, 1H, *J* = 2 Hz), 8.92 (d, 1H, *J* = 2 Hz), 8.00 (d, 1H, *J* = 9 Hz), 7.78 (br s, 1H), 7.46 (d, 1H, *J* = 3 Hz), 7.34 (dd, 1H, *J* = 9, 3 Hz), 6.67 (br s, 1H), 3.95 (s, 3H); LC-MS (LC-ES) M+H = 269.

7-Methoxy-*N*-(1-methyl-1*H*-pyrazol-3-yl)quinoline-3-carboxamide 1p.



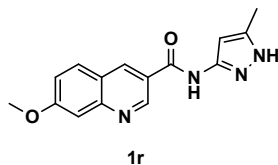
Method B; 7-Methoxyquinoline-3-carboxylic acid **7a** (Astatech); 1-Methyl-1*H*-pyrazol-3-ylamine **8k** (Oakwood); *N,N*-Dimethylformamide; 47% yield; ¹H NMR (600 MHz, CD₃SOCD₃) δ 11.10 (s, 1H), 9.30 (d, 1H, *J* = 2 Hz), 8.90 (d, 1H, *J* = 2 Hz), 7.99 (d, 1H, *J* = 9 Hz), 7.63 (d, 1H, *J* = 2 Hz), 7.46 (d, 1H, *J* = 2 Hz), 7.34 (dd, 1H, *J* = 9, 2 Hz), 6.64 (d, 1H, *J* = 2 Hz), 3.95 (s, 3H), 3.79 (s, 3H); LC-MS (LC-ES) M+H = 283.

7-Methoxy-*N*-(1-methyl-1*H*-pyrazol-5-yl)quinoline-3-carboxamide 1q.



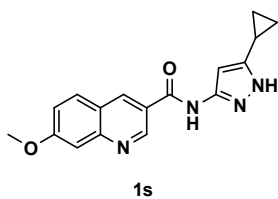
Method B; 7-Methoxyquinoline-3-carboxylic acid **7a** (Astatech); 1-Methyl-1*H*-pyrazol-4-ylamine **8l** (Oakwood); *N,N*-Dimethylformamide; 11% yield; ¹H NMR (600 MHz, CD₃SOCD₃) δ 10.62 (br s, 1H), 9.31 (s, 1H), 8.89 (s, 1H), 8.05 (d, 1H, *J* = 8 Hz), 7.49 (s, 1H), 7.42 (t, 1H, *J* = 2 Hz), 7.37 (dt, 1H, *J* = 9, 2 Hz), 6.30 (d, 1H, *J* = 2 Hz), 3.96 (s, 3H), 3.75 (s, 3H); LC-MS (LC-ES) M+H = 283.

7-Methoxy-*N*-(5-methyl-1*H*-pyrazol-3-yl)quinoline-3-carboxamide 1r.



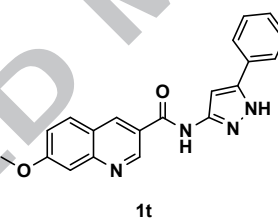
Method B; 7-Methoxyquinoline-3-carboxylic acid **7a** (Astatech); 3-Amino-5-methylpyrazole **8m** (Aldrich); *N,N*-Dimethylformamide; 9% yield; $^1\text{H NMR}$ (400 MHz, CD_3SOCD_3) δ 10.90 (br s, 1H), 9.30 (d, 1H, $J = 2$ Hz), 8.90 (d, 1H, $J = 2$ Hz), 8.15 (s, 1H), 7.99 (d, 1H, $J = 8$ Hz), 7.46 (d, 1H, $J = 2$ Hz), 7.34 (dd, 1H, $J = 9, 2$ Hz), 6.44 (br s, 1H), 3.96 (s, 3H), 2.24 (s, 3H); LC-MS (LC-ES) $\text{M}+\text{H} = 283$.

***N*-(5-Cyclopropyl-1*H*-pyrazol-3-yl)-7-methoxyquinoline-3-carboxamide 1s.**



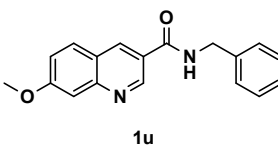
Method B; 7-Methoxyquinoline-3-carboxylic acid **7a** (Astatech); 3-Cyclopropyl-1*H*-pyrazol-5-amine **8n** (Oakwood); *N,N*-Dimethylformamide; 12% yield; $^1\text{H NMR}$ (400 MHz, CD_3SOCD_3) δ 10.90 (br s, 1H), 9.32 (d, 1H, $J = 2$ Hz), 8.94 (d, 1H, $J = 2$ Hz), 8.13 (s, 1H), 8.02 (d, 1H, $J = 8$ Hz), 7.47 (d, 1H, $J = 2$ Hz), 7.37 (dd, 1H, $J = 9, 2$ Hz), 6.34 (br s, 1H), 3.97 (s, 3H), 1.96-1.86 (m, 1H), 0.98-0.90 (m, 2H), 0.74-0.68 (m, 2H); LC-MS (LC-ES) $\text{M}+\text{H} = 309$.

7-Methoxy-*N*-(5-phenyl-1*H*-pyrazol-3-yl)quinoline-3-carboxamide 1t.



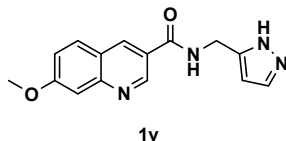
Method B; 7-Methoxyquinoline-3-carboxylic acid **7a** (Astatech); 3-Amino-5-phenylpyrazole **8o** (Aldrich); *N,N*-Dimethylformamide; 9% yield; $^1\text{H NMR}$ (400 MHz, CD_3SOCD_3) δ 12.93 (br s, 1H), 11.12 (br s, 1H), 9.34 (d, 1H, $J = 2$ Hz), 8.95 (d, 1H, $J = 2$ Hz), 8.02 (d, 1H, $J = 8$ Hz), 7.78 (d, 2H, $J = 7$ Hz), 7.48 (d, 1H, $J = 2$ Hz), 7.47 (t, 2H, $J = 7$ Hz), 7.36 (t, 1H, $J = 7$ Hz), 7.35 (dd, 1H, $J = 9, 2$ Hz), 7.08 (br s, 1H), 3.97 (s, 3H); LC-MS (LC-ES) $\text{M}+\text{H} = 345$.

***N*-Benzyl-7-methoxyquinoline-3-carboxamide 1u.**



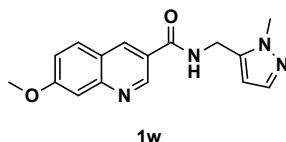
Method B; 7-Methoxyquinoline-3-carboxylic acid **7a** (Astatech); Benzylamine **8p** (Aldrich); *N,N*-Dimethylformamide; 15% yield; $^1\text{H NMR}$ (400 MHz, CD_3SOCD_3) δ 9.31 (t, 1H, $J = 6$ Hz), 9.26 (d, 1H, $J = 2$ Hz), 8.78 (d, 1H, $J = 2$ Hz), 7.99 (d, 1H, $J = 9$ Hz), 7.46 (d, 1H, $J = 2$ Hz), 7.37 (t, 2H, $J = 7$ Hz), 7.35 (d, 2H, $J = 7$ Hz), 7.32 (dd, 1H, $J = 9, 2$ Hz), 7.25 (t, 1H, $J = 7$ Hz), 4.55 (d, 2H, $J = 6$ Hz), 3.94 (s, 3H); LC-MS (LC-ES) $\text{M}+\text{H} = 293$.

***N*-((1*H*-Pyrazol-5-yl)methyl)-7-methoxyquinoline-3-carboxamide 1v.**



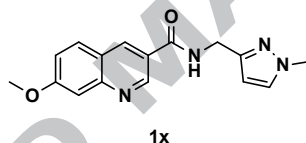
Method B; 7-Methoxyquinoline-3-carboxylic acid **7a** (Astatech); 1*H*-Pyrazole-3-methaneamine **8q** (Oakwood); *N,N*-Dimethylformamide; 43% yield; ¹H NMR (400 MHz, CD₃SOCD₃) δ 12.65 (br s, 1H), 9.23 (d, 1H, *J* = 2 Hz), 9.18 (t, 1H, *J* = 6 Hz), 8.76 (d, 1H, *J* = 2 Hz), 7.99 (d, 1H, *J* = 9 Hz), 7.59 (br s, 1H), 7.45 (d, 1H, *J* = 2 Hz), 7.32 (dd, 1H, *J* = 9, 2 Hz), 6.22 (t, 1H, *J* = 7 Hz), 4.53 (d, 2H, *J* = 6 Hz), 3.94 (s, 3H); LC-MS (LC-ES) M+H = 283.

7-Methoxy-*N*-((1-methyl-1*H*-pyrazol-5-yl)methyl)quinoline-3-carboxamide 1w.



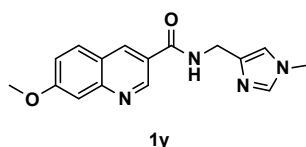
Method B; 7-Methoxyquinoline-3-carboxylic acid **7a** (Astatech); (1-Methyl-1*H*-pyrazol-5-yl)methylamine **8r** (Oakwood); *N,N*-Dimethylformamide; 32% yield; ¹H NMR (400 MHz, CD₃SOCD₃) δ 9.23 (s, 1H), 9.22 (s, 1H), 8.76 (s, 1H), 7.98 (d, 1H, *J* = 9 Hz), 7.45 (s, 1H), 7.32 (s, 2H), 6.23 (s, 1H), 4.58 (d, 2H, *J* = 6 Hz), 3.94 (s, 3H), 3.84 (s, 3H); LC-MS (LC-ES) M+H = 297.

7-Methoxy-*N*-((1-methyl-1*H*-pyrazol-3-yl)methyl)quinoline-3-carboxamide 1x.



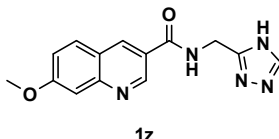
Method B; 7-Methoxyquinoline-3-carboxylic acid **7a** (Astatech); [(1-Methyl-1*H*-pyrazol-3-yl)methyl]amine **8s** (Oakwood); *N,N*-Dimethylformamide; 39% yield; ¹H NMR (400 MHz, CD₃SOCD₃) δ 9.23 (d, 1H, *J* = 2 Hz), 9.16 (t, 1H, *J* = 6 Hz), 8.76 (d, 1H, *J* = 2 Hz), 7.97 (d, 1H, *J* = 9 Hz), 7.59 (d, 1H, *J* = 2 Hz), 7.44 (d, 1H, *J* = 2 Hz), 7.32 (dd, 1H, *J* = 9, 2 Hz), 6.18 (d, 1H, *J* = 2 Hz), 4.47 (d, 2H, *J* = 6 Hz), 3.94 (s, 3H), 3.79 (s, 3H); LC-MS (LC-ES) M+H = 297.

7-Methoxy-*N*-((1-methyl-1*H*-imidazol-4-yl)methyl)quinoline-3-carboxamide 1y.



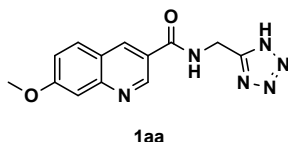
Method B; 7-Methoxyquinoline-3-carboxylic acid **7a** (Astatech); (1-Methyl-1*H*-imidazol-4-yl)methylamine **8t** (Astatech); *N,N*-Dimethylformamide; 7% yield; ¹H NMR (400 MHz, CD₃SOCD₃) δ 9.22 (d, 1H, *J* = 2 Hz), 9.34 (t, 1H, *J* = 6 Hz), 8.75 (d, 1H, *J* = 2 Hz), 7.97 (d, 1H, *J* = 9 Hz), 7.50 (d, 1H, *J* = 2 Hz), 7.44 (d, 1H, *J* = 2 Hz), 7.32 (dd, 1H, *J* = 9, 2 Hz), 7.01 (d, 1H, *J* = 2 Hz), 4.38 (d, 2H, *J* = 6 Hz), 3.94 (s, 3H), 3.60 (s, 3H); LC-MS (LC-ES) M+H = 297.

***N*-((4*H*-1,2,4-Triazol-3-yl)methyl)-7-methoxyquinoline-3-carboxamide 1z.**



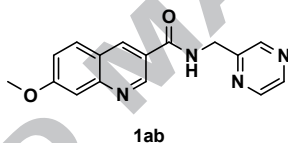
Method B; 7-Methoxyquinoline-3-carboxylic acid **7a** (Astatech); (1*H*-1,2,4-Triazol-5-ylmethyl)amine **8u** (ChemBridge); *N,N*-Dimethylformamide; 2% yield; ¹H NMR (400 MHz, CD₃SOCD₃) δ 9.50 (br s, 1H), 9.32 (br s, 1H), 9.24 (d, 1H, *J* = 2 Hz), 8.78 (d, 1H, *J* = 2 Hz), 8.19 (s, 1H), 7.99 (d, 1H, *J* = 9 Hz), 7.46 (d, 1H, *J* = 2 Hz), 7.33 (dd, 1H, *J* = 9, 2 Hz), 4.62 (s, 2H), 3.94 (s, 3H); LC-MS (LC-ES) M+H = 284.

***N*-(1*H*-Tetrazol-5-yl)methyl-7-methoxyquinoline-3-carboxamide 1aa.**



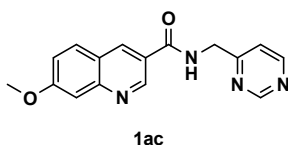
Method B; 7-Methoxyquinoline-3-carboxylic acid **7a** (Astatech); (1*H*-Tetrazol-5-ylmethyl)amine **8v** (ChemBridge); *N,N*-Dimethylformamide; 21% yield; ¹H NMR (400 MHz, CD₃SOCD₃) δ 9.48 (t, 1H, *J* = 5 Hz), 9.24 (d, 1H, *J* = 2 Hz), 8.78 (d, 1H, *J* = 2 Hz), 7.99 (d, 1H, *J* = 9 Hz), 7.46 (d, 1H, *J* = 2 Hz), 7.34 (dd, 1H, *J* = 9, 2 Hz), 4.82 (d, 2H, *J* = 6 Hz), 3.94 (s, 3H); LC-MS (LC-ES) M+H = 285.

7-Methoxy-*N*-(pyrazin-2-ylmethyl)quinoline-3-carboxamide 1ab.



Method B; 7-Methoxyquinoline-3-carboxylic acid **7a** (Astatech); 2-Aminomethylpyrazine **8w** (Oakwood); *N,N*-Dimethylformamide; 44% yield; ¹H NMR (400 MHz, CD₃SOCD₃) δ 9.46 (t, 1H, *J* = 6 Hz), 9.25 (d, 1H, *J* = 2 Hz), 8.79 (d, 1H, *J* = 2 Hz), 8.71 (d, 1H, *J* = 2 Hz), 8.61 (dd, 1H, *J* = 2, 2 Hz), 8.55 (d, 1H, *J* = 2 Hz), 7.99 (d, 1H, *J* = 9 Hz), 7.46 (d, 1H, *J* = 2 Hz), 7.33 (dd, 1H, *J* = 9, 2 Hz), 4.69 (d, 2H, *J* = 6 Hz), 3.94 (s, 3H); LC-MS (LC-ES) M+H = 295.

7-Methoxy-*N*-(pyrimidin-4-ylmethyl)quinoline-3-carboxamide 1ac.



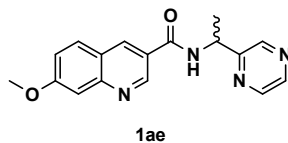
Method B; 7-Methoxyquinoline-3-carboxylic acid **7a** (Astatech); 4-(Aminomethyl)pyrimidine **8x** (Oakwood); *N,N*-Dimethylformamide; 21% yield; ¹H NMR (400 MHz, CD₃SOCD₃) δ 9.48 (t, 1H, *J* = 6 Hz), 9.28 (d, 1H, *J* = 2 Hz), 9.12 (s, 1H), 8.82 (d, 1H, *J* = 2 Hz), 8.74 (d, 1H, *J* = 5 Hz), 8.01 (d, 1H, *J* = 9 Hz), 7.52 (d, 1H, *J* = 5 Hz), 7.47 (d, 1H, *J* = 2 Hz), 7.34 (dd, 1H, *J* = 9, 2 Hz), 4.62 (d, 2H, *J* = 6 Hz), 3.94 (s, 3H); LC-MS (LC-ES) M+H = 295.

7-Methoxy-*N*-(pyrimidin-5-ylmethyl)quinoline-3-carboxamide 1ad.



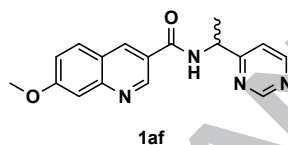
Method B; 7-Methoxyquinoline-3-carboxylic acid **7a** (Astatech); 5-Pyrimidinemethanamine **8y** (Astatech); *N,N*-Dimethylformamide; 1% yield; $^1\text{H NMR}$ (400 MHz, CD_3SOCD_3) δ 9.37 (t, 1H, $J = 6$ Hz), 9.22 (d, 1H, $J = 2$ Hz), 9.09 (s, 1H), 8.83 (s, 1H), 8.76 (d, 1H, $J = 2$ Hz), 8.20 (s, 1H), 7.99 (d, 1H, $J = 9$ Hz), 7.45 (d, 1H, $J = 2$ Hz), 7.33 (dd, 1H, $J = 9, 2$ Hz), 4.57 (d, 2H, $J = 6$ Hz), 3.94 (s, 3H); LC-MS (LC-ES) M+H = 295.

Racemic 7-Methoxy-*N*-(1-(pyrazin-2-yl)ethyl)quinoline-3-carboxamide 1ae.



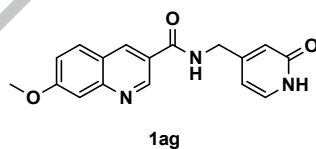
Method B; 7-Methoxyquinoline-3-carboxylic acid **7a** (Astatech); 1-Pyrazin-2-yl-ethylamine **8z** (Oakwood); *N,N*-Dimethylformamide; 49% yield; $^1\text{H NMR}$ (400 MHz, CD_3SOCD_3) δ 9.26-9.20 (m, 2H), 8.81 (d, 1H, $J = 2$ Hz), 8.76 (br s, 1H), 8.61 (dd, 1H, $J = 2, 2$ Hz), 8.54 (d, 1H, $J = 2$ Hz), 7.99 (d, 1H, $J = 9$ Hz), 7.46 (d, 1H, $J = 2$ Hz), 7.32 (dd, 1H, $J = 9, 2$ Hz), 4.14 (q, 1H, $J = 7$ Hz), 3.95 (s, 3H), 1.59 (d, 3H, $J = 7$ Hz); LC-MS (LC-ES) M+H = 309.

Racemic 7-Methoxy-*N*-(1-(pyrimidin-4-yl)ethyl)quinoline-3-carboxamide 1af.



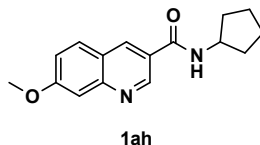
Method B; 7-Methoxyquinoline-3-carboxylic acid **7a** (Astatech); [1-(4-Pyrimidinyl)ethyl]amine **8aa** (ChemBridge); *N,N*-Dimethylformamide; 45% yield; $^1\text{H NMR}$ (400 MHz, CD_3SOCD_3) δ 9.26 (d, 1H, $J = 1$ Hz), 9.22 (d, 1H, $J = 7$ Hz), 9.14 (s, 1H), 8.82 (d, 1H, $J = 2$ Hz), 8.75 (d, 1H, $J = 5$ Hz), 8.01 (d, 1H, $J = 9$ Hz), 7.58 (dd, 1H, $J = 5, 1$ Hz), 7.47 (d, 1H, $J = 2$ Hz), 7.34 (dd, 1H, $J = 9, 2$ Hz), 4.14 (q, 1H, $J = 7$ Hz), 3.95 (s, 3H), 1.56 (d, 3H, $J = 7$ Hz); LC-MS (LC-ES) M+H = 309.

7-Methoxy-*N*-((2-oxo-1,2-dihydropyridin-4-yl)methyl)quinoline-3-carboxamide 1ag.



Method B; 7-Methoxyquinoline-3-carboxylic acid **7a** (Astatech); 4-(Aminomethyl)-2(1*H*)-pyridinone **8ab** (Astatech); *N,N*-Dimethylformamide; 27% yield; $^1\text{H NMR}$ (400 MHz, CD_3SOCD_3) δ 11.46 (br s, 1H), 9.29 (t, 1H, $J = 6$ Hz), 9.24 (d, 1H, $J = 2$ Hz), 8.79 (d, 1H, $J = 2$ Hz), 8.01 (d, 1H, $J = 9$ Hz), 7.46 (d, 1H, $J = 2$ Hz), 7.33 (dd, 1H, $J = 9, 2$ Hz), 7.32 (d, 1H, $J = 7$ Hz), 6.23 (s, 1H), 6.17 (dd, 1H, $J = 7, 1$ Hz), 4.35 (d, 2H, $J = 6$ Hz), 3.95 (s, 3H); LC-MS (LC-ES) M+H = 310.

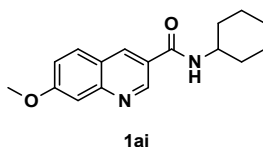
***N*-Cyclopentyl-7-methoxyquinoline-3-carboxamide 1ah.**



Commercial (Aurora Building Blocks); **Method B;** 7-Methoxyquinoline-3-carboxylic acid **7a** (Astatech); Cyclopentamine **8ac** (Aldrich); *N,N*-Dimethylformamide; 67% yield; $^1\text{H NMR}$ (400 MHz, CD_3OD) δ 9.18 (d, 1H, $J = 2$ Hz), 8.81 (d, 1H, $J = 2$ Hz), 8.06 (br s, 1H), 7.99 (d, 1H, $J = 9$ Hz), 7.42 (d, 1H, $J = 2$ Hz), 7.38 (dd, 1H, $J = 9, 2$

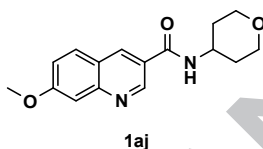
Hz), 4.42-4.32 (m, 1H), 4.00 (s, 3H), 2.14-2.02 (m, 2H), 1.86-1.76 (m, 2H), 1.72-1.56 (m, 4H); LC-MS (LC-ES) M+H = 271.

***N*-Cyclohexyl-7-methoxyquinoline-3-carboxamide 1ai.**



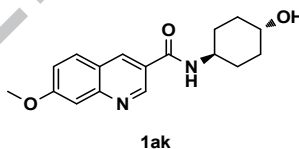
Method B; 7-Methoxyquinoline-3-carboxylic acid **7a** (Astatech); Cyclohexylamine **8ad** (Aldrich); *N,N*-Dimethylformamide; 49% yield; ¹H NMR (400 MHz, CD₃OD) δ 9.19 (d, 1H, *J* = 2 Hz), 8.83 (d, 1H, *J* = 2 Hz), 8.06 (br s, 1H), 8.00 (d, 1H, *J* = 9 Hz), 7.43 (d, 1H, *J* = 2 Hz), 7.39 (dd, 1H, *J* = 9, 2 Hz), 4.01 (s, 3H), 3.98-3.86 (m, 1H), 2.06-1.96 (m, 2H), 1.88-1.76 (m, 2H), 1.74-1.64 (m, 1H), 1.58-1.34 (m, 4H), 1.32-1.18 (m, 1H); LC-MS (LC-ES) M+H = 285.

7-Methoxy-*N*-(tetrahydro-2*H*-pyran-4-yl)quinoline-3-carboxamide 1aj.



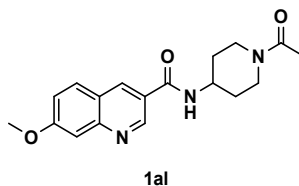
Method B; 7-Methoxyquinoline-3-carboxylic acid **7a** (Astatech); 4-Aminotetrahydropyran **8ae** (Aldrich); *N,N*-Dimethylformamide; 39% yield; ¹H NMR (400 MHz, CD₃SOCD₃) δ 9.20 (d, 1H, *J* = 2 Hz), 8.72 (d, 1H, *J* = 2 Hz), 8.59 (br s, 1H), 7.99 (d, 1H, *J* = 9 Hz), 7.44 (d, 1H, *J* = 2 Hz), 7.32 (dd, 1H, *J* = 9, 2 Hz), 4.12-4.00 (m, 1H), 3.93 (s, 3H), 3.89 (br d, 2H, *J* = 11 Hz), 3.40 (br t, 2H, *J* = 13 Hz), 1.80 (br d, 2H, *J* = 13 Hz), 1.66-1.56 (m, 2H); LC-MS (LC-ES) M+H = 287.

***N*-(trans-4-Hydroxycyclohexyl)-7-methoxyquinoline-3-carboxamide 1ak.**



Method B; 7-Methoxyquinoline-3-carboxylic acid **7a** (Astatech); trans-4-Aminocyclohexanol **8af** (Aldrich); Dichloromethane:*N,N*-Dimethylformamide (2:1); 79% yield; ¹H NMR (400 MHz, CD₃SOCD₃) δ 9.18 (d, 1H, *J* = 2 Hz), 8.72 (d, 1H, *J* = 2 Hz), 8.45 (d, 1H, *J* = 8 Hz), 7.98 (d, 1H, *J* = 9 Hz), 7.45 (d, 1H, *J* = 2 Hz), 7.32 (dd, 1H, *J* = 9, 2 Hz), 4.58 (d, 1H, *J* = 6 Hz), 3.94 (s, 3H), 3.82-3.72 (m, 1H), 3.46-3.36 (m, 1H), 1.92-1.82 (m, 4H), 1.44-1.32 (m, 2H), 1.32-1.20 (m, 2H); LC-MS (LC-ES) M+H = 301.

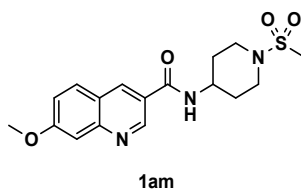
***N*-(1-Acetylpiperidin-4-yl)-7-methoxyquinoline-3-carboxamide 1al.**



Method B; 7-Methoxyquinoline-3-carboxylic acid **7a** (Astatech); 1-Acetyl-4-aminopiperidine **8ag** (Astatech); *N,N*-Dimethylformamide; 78% yield; ¹H NMR (400 MHz, CD₃OD) δ 9.14 (d, 1H, *J* = 2 Hz), 8.67 (d, 1H, *J* = 2 Hz), 8.09 (br s, 1H), 7.89 (d, 1H, *J* = 9 Hz), 7.39 (d, 1H, *J* = 2 Hz), 7.30 (dd, 1H, *J* = 9, 2 Hz), 4.58-4.48 (m, 1H), 4.24-4.12 (m,

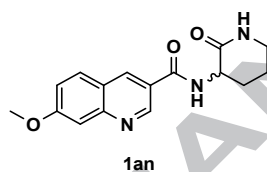
1H), 4.02-3.92 (m, 1H), 3.95 (s, 3H), 3.32-3.22 (m, 1H), 2.88-2.76 (m, 1H), 2.14-1.96 (m, 2H), 2.11 (s, 3H), 1.66-1.46 (m, 2H); LC-MS (LC-ES) M+H = 328.

7-Methoxy-*N*-(1-(methylsulfonyl)piperidin-4-yl)quinoline-3-carboxamide 1am.



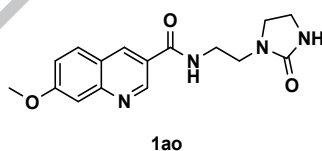
Method B; 7-Methoxyquinoline-3-carboxylic acid **7a** (Astatech); 4-Amino-1-methanesulfonylpiperidine **8ah** (Oakwood); Dichloromethane:*N,N*-Dimethylformamide (2:1); 75% yield; ¹H NMR (400 MHz, CD₃OD) δ 9.21 (d, 1H, *J* = 2 Hz), 8.73 (d, 1H, *J* = 2 Hz), 8.63 (br d, 1H, *J* = 7 Hz), 8.00 (d, 1H, *J* = 9 Hz), 7.46 (d, 1H, *J* = 2 Hz), 7.33 (dd, 1H, *J* = 9, 2 Hz), 4.06-3.92 (m, 1H), 3.95 (s, 3H), 3.64-3.54 (m, 2H), 2.94-2.84 (m, 2H), 2.88 (s, 3H), 2.02-1.92 (m, 2H), 1.70-1.54 (m, 2H); LC-MS (LC-ES) M+H = 364.

7-Methoxy-*N*-(2-oxopiperidin-3-yl)quinoline-3-carboxamide 1an.



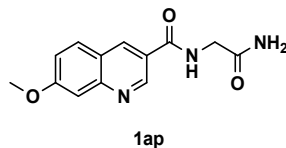
Method B; 7-Methoxyquinoline-3-carboxylic acid **7a** (Astatech); 3-Aminopiperidin-2-one **8ai** (Aldrich); *N,N*-Dimethylformamide; 56% yield; ¹H NMR (400 MHz, CD₃OD) δ 9.22 (d, 1H, *J* = 2 Hz), 8.91 (d, 1H, *J* = 8 Hz), 8.75 (br d, 1H, *J* = 2 Hz), 7.99 (d, 1H, *J* = 9 Hz), 7.69 (br s, 1H), 7.46 (d, 1H, *J* = 2 Hz), 7.33 (dd, 1H, *J* = 9, 2 Hz), 4.48-4.42 (m, 1H), 3.95 (s, 3H), 3.22-3.14 (m, 2H), 2.10-2.02 (m, 1H), 1.90-1.76 (m, 3H); LC-MS (LC-ES) M+H = 300.

7-Methoxy-*N*-(2-(2-oxoimidazolidin-1-yl)ethyl)quinoline-3-carboxamide 1ao.

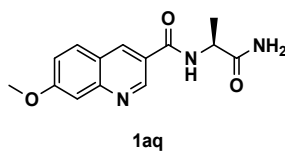


Method B; 7-Methoxyquinoline-3-carboxylic acid **7a** (Astatech); 1-(2-Aminoethyl)-2-imidazolidinone **8aj** (Oakwood); *N,N*-Dimethylformamide; 34% yield; ¹H NMR (400 MHz, CD₃OD) δ 9.18 (d, 1H, *J* = 2 Hz), 8.81 (t, 1H, *J* = 6 Hz), 8.69 (d, 1H, *J* = 2 Hz), 7.98 (d, 1H, *J* = 9 Hz), 7.45 (d, 1H, *J* = 2 Hz), 7.32 (dd, 1H, *J* = 9, 2 Hz), 6.29 (br s, 1H), 3.95 (s, 3H), 3.46-3.88 (m, 4H), 3.26 (t, 2H, *J* = 7 Hz), 3.22 (t, 2H, *J* = 7 Hz); LC-MS (LC-ES) M+H = 315.

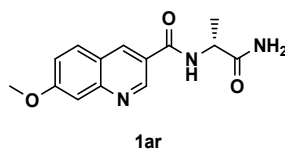
***N*-(2-Amino-2-oxoethyl)-7-methoxyquinoline-3-carboxamide 1ap.**



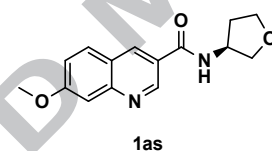
Method B; 7-Methoxyquinoline-3-carboxylic acid **7a** (Astatech); 2-Aminoacetamide **8ak** (Aldrich); *N,N*-Dimethylformamide; 52% yield; ¹H NMR (400 MHz, CD₃SOCD₃) δ 9.24 (d, 1H, *J* = 2 Hz), 8.92 (t, 1H, *J* = 6 Hz), 8.76 (d, 1H, *J* = 2 Hz), 7.99 (d, 1H, *J* = 9 Hz), 7.46 (d, 1H, *J* = 2 Hz), 7.42 (br s, 1H), 7.33 (dd, 1H, *J* = 9, 2 Hz), 7.06 (br s, 1H), 3.95 (s, 3H), 3.88 (d, 2H, *J* = 6 Hz); LC-MS (LC-ES) M+H = 260.

(S)-N-(1-Amino-1-oxopropan-2-yl)-7-methoxyquinoline-3-carboxamide 1aq.

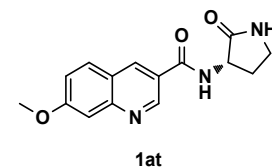
Method A; 7-Methoxyquinoline-3-carboxylic acid **7a** (Astatech); (*S*)-2-Aminopropanamide **8al** (Aldrich); dichloromethane; 56% yield; ¹H NMR (400 MHz, CD₃SOCD₃) δ 9.23 (d, 1H, *J* = 2 Hz), 8.79 (d, 1H, *J* = 2 Hz), 8.73 (d, 1H, *J* = 8 Hz), 7.98 (d, 1H, *J* = 9 Hz), 7.45 (d, 1H, *J* = 2 Hz), 7.45 (br s, 1H), 7.32 (dd, 1H, *J* = 9, 2 Hz), 7.03 (br s, 1H), 4.46 (p, 1H, *J* = 7 Hz), 3.94 (s, 3H), 1.36 (d, 3H, *J* = 7 Hz); LC-MS (LC-ES) M+H = 274.

(R)-N-(1-Amino-1-oxopropan-2-yl)-7-methoxyquinoline-3-carboxamide 1ar.

Method B; 7-Methoxyquinoline-3-carboxylic acid **7a** (Astatech); (*R*)-2-Aminopropanamide **8am** (Aldrich); *N,N*-Dimethylformamide; 47% yield; ¹H NMR (400 MHz, CD₃SOCD₃) δ 9.23 (d, 1H, *J* = 2 Hz), 8.79 (d, 1H, *J* = 2 Hz), 8.67 (d, 1H, *J* = 8 Hz), 7.98 (d, 1H, *J* = 9 Hz), 7.45 (d, 1H, *J* = 2 Hz), 7.41 (br s, 1H), 7.32 (dd, 1H, *J* = 9, 2 Hz), 6.98 (br s, 1H), 4.46 (p, 1H, *J* = 7 Hz), 3.94 (s, 3H), 1.36 (d, 3H, *J* = 7 Hz); LC-MS (LC-ES) M+H = 274.

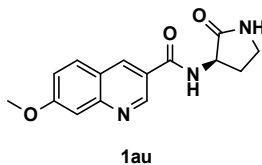
(S)-7-Methoxy-N-(tetrahydrofuran-3-yl)quinoline-3-carboxamide 1as.

Method B; 7-Methoxyquinoline-3-carboxylic acid **7a** (Astatech); (*S*)-tetrahydrofuran-3-amine **8an** (Aldrich); *N,N*-Dimethylformamide; 72% yield; ¹H NMR (400 MHz, CD₃SOCD₃) δ 9.21 (d, 1H, *J* = 2 Hz), 8.77 (br d, 1H, *J* = 7 Hz), 8.74 (d, 1H, *J* = 2 Hz), 7.98 (d, 1H, *J* = 9 Hz), 7.45 (d, 1H, *J* = 2 Hz), 7.33 (dd, 1H, *J* = 9, 2 Hz), 4.58-4.46 (m, 1H), 3.95 (s, 3H), 3.92-3.84 (m, 2H), 3.74 (dt, 1H, *J* = 9, 7 Hz), 3.64 (dd, 1H, *J* = 9, 4 Hz), 2.26-2.14 (m, 1H), 2.02-1.90 (m, 1H); LC-MS (LC-ES) M+H = 273.

(S)-7-Methoxy-N-(2-oxopyrrolidin-3-yl)quinoline-3-carboxamide 1at.

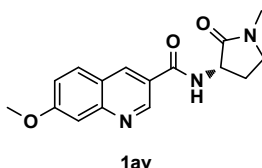
Method B; 7-Methoxyquinoline-3-carboxylic acid **7a** (Astatech); 3-Amino-2-pyrrolidinone **8ao** (Astatech); *N,N*-Dimethylformamide; 53% yield; Separation of enantiomers on a Chiralpak® IB column (1:3 ethanol:heptane, 1.0 mL/min, 25 minutes, *t_R* = 11.7 minutes); ¹H NMR (400 MHz, CD₃OD) δ 9.22 (d, 1H, *J* = 2 Hz), 8.76 (d, 1H, *J* = 2 Hz), 7.96 (d, 1H, *J* = 9 Hz), 7.46 (d, 1H, *J* = 2 Hz), 7.36 (dd, 1H, *J* = 9, 2 Hz), 4.02 (s, 3H), 4.80-4.72 (m, 1H), 3.48-3.32 (m, 2H), 2.64-2.52 (m, 1H), 2.28-2.12 (m, 1H); LC-MS (LC-ES) M+H = 286.

(R)-7-Methoxy-N-(2-oxopyrrolidin-3-yl)quinoline-3-carboxamide 1au.



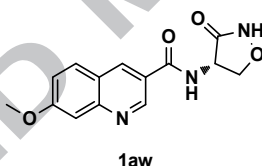
Method B; 7-Methoxyquinoline-3-carboxylic acid **7a** (Astatech); 3-Amino-2-pyrrolidinone **8ap** (Astatech); *N,N*-Dimethylformamide; 53% yield; Separation of enantiomers on a Chiralpak® IB column (1:3 ethanol:heptane, 1.0 mL/min, 25 minutes, t_R = 16.6 minutes); $^1\text{H NMR}$ (400 MHz, CD_3OD) δ 9.22 (d, 1H, J = 2 Hz), 8.76 (d, 1H, J = 2 Hz), 7.96 (d, 1H, J = 9 Hz), 7.46 (d, 1H, J = 2 Hz), 7.36 (dd, 1H, J = 9, 2 Hz), 4.02 (s, 3H), 4.80-4.72 (m, 1H), 3.48-3.32 (m, 2H), 2.64-2.52 (m, 1H), 2.28-2.12 (m, 1H); LC-MS (LC-ES) $M+H$ = 286.

(S)-7-Methoxy-*N*-(1-methyl-2-oxopyrrolidin-3-yl)quinoline-3-carboxamide 1av.



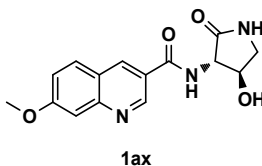
Method B; 7-Methoxyquinoline-3-carboxylic acid **7a** (Astatech); (*S*)-3-amino-1-methylpyrrolidin-2-one **8aq** (PharmaBlock); *N,N*-Dimethylformamide; 17% yield; $^1\text{H NMR}$ (400 MHz, CD_3OD) δ 9.17 (d, 1H, J = 2 Hz), 8.70 (d, 1H, J = 2 Hz), 7.91 (d, 1H, J = 9 Hz), 7.41 (d, 1H, J = 2 Hz), 7.31 (dd, 1H, J = 9, 2 Hz), 4.74 (t, 1H, J = 7 Hz), 3.98 (s, 3H), 3.52-3.44 (m, 2H), 2.91 (s, 3H), 2.60-2.48 (m, 1H), 2.18-2.04 (m, 1H); LC-MS (LC-ES) $M+H$ = 300.

(S)-7-Methoxy-*N*-(3-oxoisoxazolidin-4-yl)quinoline-3-carboxamide 1aw.



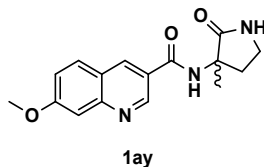
Method B; 7-Methoxyquinoline-3-carboxylic acid **7a** (Astatech); *L*-Cycloserine **8ar** (Aldrich); *N,N*-Dimethylformamide; 28% yield; $^1\text{H NMR}$ (400 MHz, CD_3SOCD_3) δ 11.62 (br s, 1H), 9.22 (d, 1H, J = 2 Hz), 8.77 (d, 1H, J = 2 Hz), 8.13 (br s, 1H), 8.00 (d, 1H, J = 9 Hz), 7.46 (d, 1H, J = 2 Hz), 7.34 (dd, 1H, J = 9, 2 Hz), 5.40 (q, 1H, J = 7 Hz), 4.62 (t, 1H, J = 7 Hz), 4.16 (t, 1H, J = 7 Hz), 3.95 (s, 3H); LC-MS (LC-ES) $M+H$ = 288.

***N*-((3*S*,4*R*)-4-Hydroxy-2-oxopyrrolidin-3-yl)-7-methoxyquinoline-3-carboxamide 1ax.**



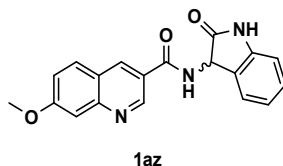
Method B; 7-Methoxyquinoline-3-carboxylic acid **7a** (Astatech); (3*S*,4*R*)-3-Amino-4-hydroxypyrrolidin-2-one **8as**; $^{40}\text{N,N}$ -Dimethylformamide; 51% yield; $^1\text{H NMR}$ (400 MHz, CD_3SOCD_3) δ 9.24 (d, 1H, J = 2 Hz), 8.95 (br d, 1H, J = 8 Hz), 8.76 (d, 1H, J = 2 Hz), 8.01 (d, 1H, J = 9 Hz), 7.81 (br s, 1H), 7.47 (d, 1H, J = 2 Hz), 7.34 (dd, 1H, J = 9, 2 Hz), 5.56 (d, 1H, J = 5 Hz), 4.46-4.34 (m, 2H), 3.96 (s, 3H), 3.50-3.44 (m, 1H), 3.04-2.96 (m, 1H); LC-MS (LC-ES) $M+H$ = 302.

Racemic 7-Methoxy-*N*-(3-methyl-2-oxopyrrolidin-3-yl)quinoline-3-carboxamide 1ay.



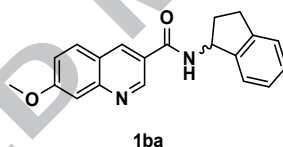
Method B; 7-Methoxyquinoline-3-carboxylic acid **7a** (Astatech); 3-Amino-3-methylpyrrolidin-2-one **8at**;⁴¹ Dichloromethane:*N,N*-Dimethylformamide (1:1); 18% yield; ¹H NMR (400 MHz, CD₃OD) δ 9.16 (d, 1H, *J* = 2 Hz), 8.73 (d, 1H, *J* = 2 Hz), 8.06 (br s, 1H), 7.92 (d, 1H, *J* = 9 Hz), 7.41 (d, 1H, *J* = 2 Hz), 7.32 (dd, 1H, *J* = 9, 2 Hz), 3.98 (s, 3H), 3.50 (dt, 1H, *J* = 9, 2 Hz), 3.40 (dt, 1H, *J* = 9, 7 Hz), 2.79 (dt, 1H, *J* = 9, 7 Hz), 2.17 (ddd, 1H, *J* = 9, 7, 2 Hz), 1.52 (s, 3H); LC-MS (LC-ES) M+H = 300.

7-Methoxy-*N*-(2-oxoindolin-3-yl)quinoline-3-carboxamide 1az.



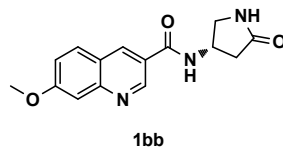
Method B; 7-Methoxyquinoline-3-carboxylic acid **7a** (Astatech); 3-Aminoindolin-2-one **8au** (Astatech); *N,N*-Dimethylformamide; 63% yield; ¹H NMR (400 MHz, CD₃OD) δ 9.21 (d, 1H, *J* = 2 Hz), 8.75 (br s, 1H), 7.94 (d, 1H, *J* = 9 Hz), 7.81 (br s, 1H), 7.43 (d, 1H, *J* = 2 Hz), 7.34 (dd, 1H, *J* = 9, 2 Hz), 7.32-7.22 (m, 2H), 7.03 (t, 1H, *J* = 7 Hz), 6.93 (d, 1H, *J* = 7 Hz), 5.46 (s, 1H), 3.98 (s, 3H); LC-MS (LC-ES) M+H = 334.

***N*-(2,3-Dihydro-1*H*-inden-1-yl)-7-(methoxy)-3-quinolinecarboxamide 1ba.**



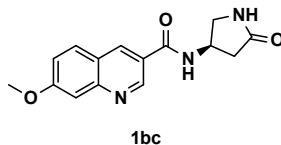
Method B; 7-Methoxyquinoline-3-carboxylic acid **7a** (Astatech); 1-Aminoindane **8av** (Aldrich); *N,N*-Dimethylformamide; 82% yield; ¹H NMR (400 MHz, CDCl₃) δ 9.20 (d, 1H, *J* = 2 Hz), 8.67 (d, 1H, *J* = 2 Hz), 8.16 (br s, 1H), 7.81 (d, 1H, *J* = 9 Hz), 7.49 (d, 1H, *J* = 2 Hz), 7.39 (br d, 1H, *J* = 7 Hz), 7.29 (dd, 1H, *J* = 9, 2 Hz), 7.28-7.20 (m, 2H), 6.82 (br d, 1H, *J* = 7 Hz), 5.75 (q, 1H, *J* = 7 Hz), 3.97 (s, 3H), 3.14-3.02 (m, 1H), 3.00-2.90 (m, 1H), 2.78-2.66 (m, 1H), 2.08-1.96 (m, 1H); LC-MS (LC-ES) M+H = 319.

(*S*)-7-Methoxy-*N*-(5-oxopyrrolidin-3-yl)quinoline-3-carboxamide 1bb.



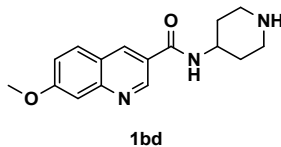
Method B; 7-Methoxyquinoline-3-carboxylic acid **7a** (Astatech); 4-Aminopyrrolidin-2-one **8aw** (Fluorochem); *N,N*-Dimethylformamide; Separation of enantiomers on a Chiralcel® OJ column (1:4 ethanol:heptane, 1.0 mL/min, 30 minutes, *t_R* = 10.6 minutes); 56% yield; ¹H NMR (400 MHz, CD₃OD) δ 9.16 (d, 1H, *J* = 2 Hz), 8.73 (d, 1H, *J* = 2 Hz), 8.06 (br s, 1H), 7.92 (d, 1H, *J* = 9 Hz), 7.39 (d, 1H, *J* = 2 Hz), 7.32 (dd, 1H, *J* = 9, 2 Hz), 4.86-4.74 (m, 1H), 3.97 (s, 3H), 3.83 (dd, 1H, *J* = 9, 7 Hz), 3.41 (dd, 1H, *J* = 9, 4 Hz), 2.79 (dd, 1H, *J* = 13, 7 Hz), 2.47 (dd, 1H, *J* = 13, 4 Hz); LC-MS (LC-ES) M+H = 286.

(*R*)-7-Methoxy-*N*-(5-oxopyrrolidin-3-yl)quinoline-3-carboxamide 1bc.



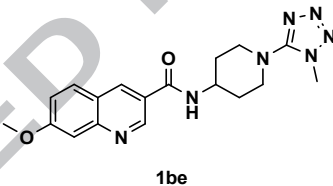
Method B; 7-Methoxyquinoline-3-carboxylic acid **7a** (Astatech); 4-Aminopyrrolidin-2-one **8ax** (Fluorochem); *N,N*-Dimethylformamide; Separation of enantiomers on a Chiralcel® OJ column (1:4 ethanol:heptane, 1.0 mL/min, 30 minutes, $t_R = 15.9$ minutes); 56% yield; $^1\text{H NMR}$ (400 MHz, CD_3OD) δ 9.16 (d, 1H, $J = 2$ Hz), 8.73 (d, 1H, $J = 2$ Hz), 8.06 (br s, 1H), 7.92 (d, 1H, $J = 9$ Hz), 7.39 (d, 1H, $J = 2$ Hz), 7.32 (dd, 1H, $J = 9, 2$ Hz), 4.86-4.74 (m, 1H), 3.97 (s, 3H), 3.83 (dd, 1H, $J = 9, 7$ Hz), 3.41 (dd, 1H, $J = 9, 4$ Hz), 2.79 (dd, 1H, $J = 13, 7$ Hz), 2.47 (dd, 1H, $J = 13, 4$ Hz); LC-MS (LC-ES) $M+H = 286$.

7-Methoxy-*N*-(piperidin-4-yl)quinoline-3-carboxamide 1bd.



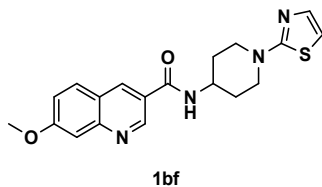
Method B; 7-Methoxyquinoline-3-carboxylic acid **7a** (Astatech); 4-Amino-1-*N*-Boc-piperidine **8ay** (Astatech); *N,N*-Dimethylformamide; Followed by hydrochloric acid in 1,4-dioxane cleavage of the tert-butyloxycarbonyl protecting group; 82% yield; $^1\text{H NMR}$ (400 MHz, CD_3OD) δ 9.57 (br s, 1H), 9.50 (br s, 1H), 8.34 (d, 1H, $J = 2$ Hz), 8.01 (br s, 2H), 7.66 (d, 1H, $J = 2$ Hz), 7.58 (br s, 1H), 4.34-4.22 (m, 1H), 4.12 (s, 3H), 3.58-3.48 (d, 2H, $J = 12$ Hz), 3.18 (t, 2H, $J = 12$ Hz), 2.26 (d, 2H, $J = 13$ Hz), 2.12-1.96 (m, 2H); LC-MS (LC-ES) $M+H = 286$.

7-Methoxy-*N*-(1-(1-methyl-1H-tetrazol-5-yl)piperidin-4-yl)quinoline-3-carboxamide 1be.

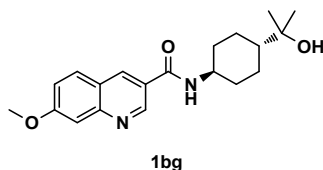


Method B; 7-Methoxyquinoline-3-carboxylic acid **7a** (Astatech); 1-(1-Methyl-1H-tetrazol-5-yl)piperidin-4-amine **8az** (Enamine); *N,N*-Dimethylformamide; 82% yield; $^1\text{H NMR}$ (400 MHz, CDCl_3) δ 9.22 (d, 1H, $J = 2$ Hz), 8.57 (d, 1H, $J = 2$ Hz), 7.81 (d, 1H, $J = 9$ Hz), 7.42 (d, 1H, $J = 2$ Hz), 7.25 (dd, 1H, $J = 9, 2$ Hz), 6.74 (d, 1H, $J = 8$ Hz), 4.42-4.19 (m, 1H), 3.97 (s, 3H), 3.90 (s, 3H), 3.68 (d, 2H, $J = 13$ Hz), 3.37-3.17 (m, 2H), 2.26-2.10 (m, 2H), 1.95-1.76 (m, 2H); LC-MS (LC-ES) $M+H = 368$.

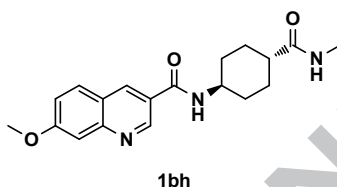
7-Methoxy-*N*-(1-(thiazol-2-yl)piperidin-4-yl)quinoline-3-carboxamide 1bf.



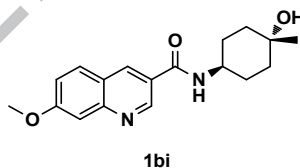
Method B; 7-Methoxyquinoline-3-carboxylic acid **7a** (Astatech); 1-(1,3-thiazol-2-yl)piperidin-4-amine **8ba** (PharmaBlock); Dichloromethane:*N,N*-Dimethylformamide (3:1); 34% yield; $^1\text{H NMR}$ (400 MHz, CDCl_3) δ 9.21 (d, 1H, $J = 2$ Hz), 8.73 (d, 1H, $J = 2$ Hz), 8.56 (d, 1H, $J = 7$ Hz), 7.98 (d, 1H, $J = 9$ Hz), 7.45 (d, 1H, $J = 2$ Hz), 7.32 (dd, 1H, $J = 9, 2$ Hz), 7.16 (d, 1H, $J = 4$ Hz), 6.83 (d, 1H, $J = 4$ Hz), 4.20-4.06 (m, 1H), 3.95 (s, 3H), 3.94 (d, 2H, $J = 13$ Hz), 3.18 (br t, 2H, $J = 12$ Hz), 1.95 (br d, 2H, $J = 12$ Hz), 1.68 (br q, 2H, $J = 12$ Hz); LC-MS (LC-ES) $M+H = 369$.

***N*-(trans-4-(2-Hydroxypropan-2-yl)cyclohexyl)-7-methoxyquinoline-3-carboxamide 1bg.**

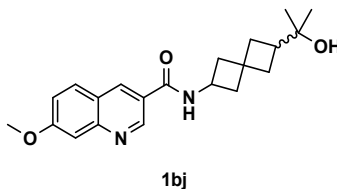
Method B; 7-Methoxyquinoline-3-carboxylic acid **7a** (Astatech); 2-(trans-4-Aminocyclohexyl)propan-2-ol **8bb** (PharmaBlock); Dichloromethane:*N,N*-Dimethylformamide (1.6:1); 71% yield; ¹H NMR (400 MHz, CD₃SOCD₃) δ 9.27 (d, 1H, *J* = 2 Hz), 8.91 (d, 1H, *J* = 2 Hz), 8.56 (d, 1H, *J* = 8 Hz), 8.08 (d, 1H, *J* = 9 Hz), 7.48 (d, 1H, *J* = 2 Hz), 7.40 (dd, 1H, *J* = 9, 2 Hz), 3.97 (s, 3H), 3.77 (dtt, 1H, *J* = 12, 8, 4 Hz), 1.96 (br d, 2H, *J* = 13 Hz), 1.85 (br d, 2H, *J* = 11 Hz), 1.33 (q, 2H, *J* = 12 Hz), 1.26-1.06 (m, 3H), 1.05 (s, 6H); LC-MS (LC-ES) M+H = 343.

7-Methoxy-*N*-(trans-4-(methylcarbamoyl)cyclohexyl)quinoline-3-carboxamide 1bh.

Method B; 7-Methoxyquinoline-3-carboxylic acid **7a** (Astatech); trans-4-Amino-*N*-methylcyclohexanecarboxamide **8bc** (BOC Sciences); Dichloromethane; 31% yield; ¹H NMR (400 MHz, CD₃SOCD₃) δ 9.11 (d, 1H, *J* = 2 Hz), 8.70 (d, 1H, *J* = 2 Hz), 8.44 (d, 1H, *J* = 8 Hz), 7.98 (d, 1H, *J* = 9 Hz), 7.63 (br q, 1H, *J* = 5 Hz), 7.45 (d, 1H, *J* = 2 Hz), 7.31 (dd, 1H, *J* = 9, 2 Hz), 3.95 (s, 3H), 3.86-3.72 (m, 1H), 2.57 (d, 3H, *J* = 5 Hz), 2.08 (tt, 1H, *J* = 15, 3 Hz), 1.94 (br d, 2H, *J* = 13 Hz), 1.79 (br d, 2H, *J* = 12 Hz), 1.47 (br q, 2H, *J* = 13 Hz), 1.37 (br q, 2H, *J* = 13 Hz); LC-MS (LC-ES) M+H = 342.

***N*-(trans-4-Hydroxy-4-methylcyclohexyl)-7-methoxyquinoline-3-carboxamide 1bi.**

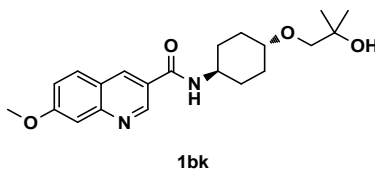
Method A; 7-Methoxyquinoline-3-carboxylic acid **7a** (Astatech); trans-4-Amino-1-methylcyclohexanol **8bd** (Enamine); 1,4-Dioxane; 49% yield; ¹H NMR (400 MHz, CD₃SOCD₃) δ 9.17 (d, 1H, *J* = 2 Hz), 8.69 (d, 1H, *J* = 2 Hz), 8.41 (d, 1H, *J* = 8 Hz), 7.98 (d, 1H, *J* = 9 Hz), 7.44 (d, 1H, *J* = 2 Hz), 7.31 (dd, 1H, *J* = 9, 2 Hz), 4.29 (s, 1H), 3.94 (s, 3H), 3.92-3.80 (m, 1H), 1.86-1.76 (m, 2H), 1.66-1.56 (m, 2H), 1.56-1.40 (m, 4H), 1.16 (s, 3H); LC-MS (LC-ES) M+H = 315.

***N*-(6-(2-Hydroxypropan-2-yl)spiro[3.3]heptan-2-yl)-7-methoxyquinoline-3-carboxamide 1bj.**

Method A; 7-Methoxyquinoline-3-carboxylic acid **7a** (Astatech); 2-(6-Aminospiro[3.3]heptan-2-yl)propan-2-ol **8be**; ⁴¹ 1,4-Dioxane; 74% yield; ¹H NMR (400 MHz, CD₃SOCD₃) δ 9.18 (d, 1H, *J* = 2 Hz), 8.77 (d, 1H, *J* = 7 Hz),

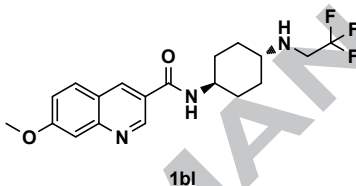
8.70 (t, 1H, $J = 2$ Hz), 7.97 (d, 1H, $J = 9$ Hz), 7.44 (d, 1H, $J = 2$ Hz), 7.31 (dd, 1H, $J = 9, 2$ Hz), 4.33 (h, 1H, $J = 8$ Hz), 3.99 (s, 1H), 3.94 (s, 3H), 2.46-2.36 (m, 1H), 2.22-2.12 (m, 1H), 2.11 (q, 2H, $J = 9$ Hz), 2.04-1.86 (m, 4H), 1.76-1.66 (m, 1H), 0.96 (s, 3H), 0.94 (s, 3H); LC-MS (LC-ES) M+H = 355.

***N*-(trans-4-(2-Hydroxy-2-methylpropoxy)cyclohexyl)-7-methoxyquinoline-3-carboxamide 1bk.**



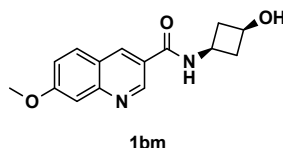
Method A; 7-Methoxyquinoline-3-carboxylic acid **7a** (Astatech); 1-((trans-4-Aminocyclohexyl)oxy)-2-methylpropan-2-ol **8bf**;⁴¹ 1,4-Dioxane; 50% yield; ¹H NMR (400 MHz, CD₃SOCD₃) δ 9.18 (d, 1H, $J = 2$ Hz), 8.69 (d, 1H, $J = 2$ Hz), 8.45 (d, 1H, $J = 8$ Hz), 7.98 (d, 1H, $J = 9$ Hz), 7.44 (d, 1H, $J = 2$ Hz), 7.31 (dd, 1H, $J = 9, 2$ Hz), 4.21 (s, 1H), 3.94 (s, 3H), 3.81 (qt, 1H, $J = 8, 4$ Hz), 3.28-3.18 (m, 1H), 3.17 (s, 2H), 2.02 (br d, 2H, $J = 10$ Hz), 1.90 (br d, 2H, $J = 10$ Hz), 1.39 (q, 2H, $J = 13$ Hz), 1.26 (q, 2H, $J = 13$ Hz), 1.06 (s, 6H); LC-MS (LC-ES) M+H = 373.

7-Methoxy-*N*-(trans-4-((2,2,2-trifluoroethyl)amino)cyclohexyl)quinoline-3-carboxamide 1bl.



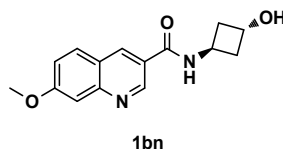
Method A; 7-Methoxyquinoline-3-carboxylic acid **7a** (Astatech); trans-*N*1-(2,2,2-Trifluoroethyl)cyclohexane-1,4-diamine **8bg**;⁴¹ 1,4-Dioxane; 43% yield; ¹H NMR (400 MHz, CD₃SOCD₃) δ 9.18 (d, 1H, $J = 2$ Hz), 8.69 (d, 1H, $J = 2$ Hz), 8.45 (d, 1H, $J = 8$ Hz), 7.97 (d, 1H, $J = 9$ Hz), 7.44 (d, 1H, $J = 2$ Hz), 7.31 (dd, 1H, $J = 9, 2$ Hz), 3.94 (s, 3H), 3.78 (qt, 1H, $J = 8, 4$ Hz), 3.30-3.18 (m, 2H), 2.48-2.36 (m, 1H), 2.20 (q, 1H, $J = 8$ Hz), 1.91 (br t, 4H, $J = 14$ Hz), 1.36 (q, 2H, $J = 12$ Hz), 1.11 (q, 2H, $J = 14$ Hz); LC-MS (LC-ES) M+H = 382.

***N*-((1*s*,3*s*)-3-Hydroxycyclobutyl)-7-methoxyquinoline-3-carboxamide 1bm.**



Method B; 7-Methoxyquinoline-3-carboxylic acid **7a** (Astatech); cis-3-Aminocyclobutanol **8bh** (Astatech); *N,N*-Dimethylformamide; 21% yield; ¹H NMR (400 MHz, CD₃SOCD₃) δ 9.18 (d, 1H, $J = 2$ Hz), 8.79 (d, 1H, $J = 7$ Hz), 8.71 (d, 1H, $J = 2$ Hz), 7.97 (d, 1H, $J = 9$ Hz), 7.44 (d, 1H, $J = 2$ Hz), 7.32 (dd, 1H, $J = 9, 2$ Hz), 5.14 (br s, 1H), 4.02-3.90 (m, 1H), 3.94 (s, 3H), 3.88 (p, 1H, $J = 8$ Hz), 2.64-2.54 (m, 2H), 2.00-1.88 (m, 2H); LC-MS (LC-ES) M+H = 273.

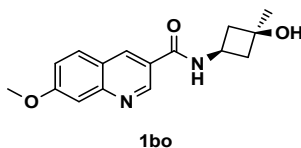
***N*-((1*r*,3*r*)-3-Hydroxycyclobutyl)-7-methoxyquinoline-3-carboxamide 1bn.**



Method B; 7-Methoxyquinoline-3-carboxylic acid **7a** (Astatech); trans-3-Aminocyclobutanol **8bi** (Astatech); *N,N*-Dimethylformamide; 36% yield; ¹H NMR (400 MHz, CD₃SOCD₃) δ 9.19 (d, 1H, $J = 2$ Hz), 8.80 (d, 1H, $J = 7$ Hz),

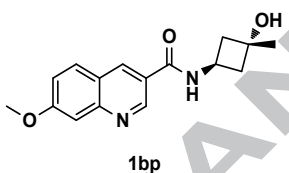
8.71 (d, 1H, $J = 2$ Hz), 7.97 (d, 1H, $J = 9$ Hz), 7.44 (d, 1H, $J = 2$ Hz), 7.32 (dd, 1H, $J = 9, 2$ Hz), 5.14 (br s, 1H), 4.02-3.90 (m, 1H), 3.94 (s, 3H), 3.88 (p, 1H, $J = 8$ Hz), 2.64-2.54 (m, 2H), 2.00-1.90 (m, 2H); LC-MS (LC-ES) M+H = 273.

***N*-((1*s*,3*s*)-3-Hydroxy-3-methylcyclobutyl)-7-methoxyquinoline-3-carboxamide 1bo.**



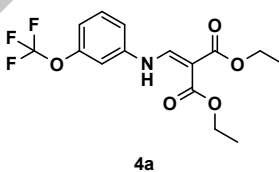
Method A; 7-Methoxyquinoline-3-carboxylic acid **7a** (Astatech); *cis*-3-Amino-1-methylcyclobutanol **8bj** (Astatech); 1,4-Dioxane; 26% yield; $^1\text{H NMR}$ (400 MHz, CD_3SOCD_3) δ 9.19 (d, 1H, $J = 2$ Hz), 8.82 (d, 1H, $J = 7$ Hz), 8.72 (d, 1H, $J = 2$ Hz), 7.97 (d, 1H, $J = 9$ Hz), 7.44 (d, 1H, $J = 2$ Hz), 7.31 (dd, 1H, $J = 9, 2$ Hz), 4.98 (s, 1H), 4.02 (h, 1H, $J = 8$ Hz), 3.94 (s, 3H), 2.36-2.28 (m, 2H), 2.16-2.10 (m, 2H), 1.28 (s, 3H); LC-MS (LC-ES) M+H = 287.

***N*-((1*r*,3*r*)-3-Hydroxy-3-methylcyclobutyl)-7-methoxyquinoline-3-carboxamide 1bp.**



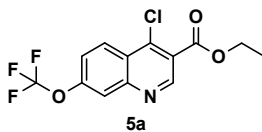
Method A; 7-Methoxyquinoline-3-carboxylic acid **7a** (Astatech); *trans*-3-Amino-1-methylcyclobutanol **8bk** (Astatech); 1,4-Dioxane; 25% yield; $^1\text{H NMR}$ (400 MHz, CD_3SOCD_3) δ 9.18 (d, 1H, $J = 2$ Hz), 8.79 (d, 1H, $J = 7$ Hz), 8.70 (d, 1H, $J = 2$ Hz), 7.98 (d, 1H, $J = 9$ Hz), 7.44 (d, 1H, $J = 2$ Hz), 7.31 (dd, 1H, $J = 9, 2$ Hz), 4.86 (s, 1H), 4.54 (h, 1H, $J = 8$ Hz), 3.94 (s, 3H), 2.34-2.26 (m, 2H), 2.12-2.06 (m, 2H), 1.29 (s, 3H); LC-MS (LC-ES) M+H = 287.

Diethyl 2-(((3-(trifluoromethoxy)phenyl)amino)methylene)malonate 4a



Diethyl 2-(ethoxymethylene)malonate **3** (5.70 mL, 28.2 mmol) was added to 3-(trifluoromethoxy)aniline **2a** (3.77 mL, 28.2 mmol) in toluene (30 mL) and the reaction mixture was heated in a sealed tube at 120 °C for eighteen hours, then concentrated to give diethyl 2-(((3-(trifluoromethoxy)phenyl)amino)methylene)malonate **4a** (10.0 g, 28.8 mmol, 99% yield) as a dark red syrup. $^1\text{H NMR}$ (400 MHz, CDCl_3) δ 11.05 (d, 1H, $J = 14$ Hz), 8.47 (d, 1H, $J = 13$ Hz), 7.44-7.37 (m, 1H), 7.07 (ddd, 1H, $J = 8, 2, 1$ Hz), 7.04-6.96 (m, 2H), 4.32 (q, 2H, $J = 7$ Hz), 4.27 (q, 2H, $J = 7$ Hz), 1.39 (t, 3H, $J = 7$ Hz), 1.34 (t, 3H, $J = 7$ Hz); LC-MS (LC-ES) M+H = 348.

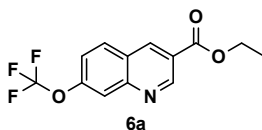
Ethyl 4-chloro-7-(trifluoromethoxy)quinoline-3-carboxylate 5a



Phosphorus oxychloride (30.2 mL, 324 mmol) was added to diethyl 2-(((3-(trifluoromethoxy)phenyl)amino)methylene)malonate **4a** (9.00 g, 25.9 mmol) and the reaction mixture was heated in a sealed tube at 115 °C. After three hours, the temperature was increased to 125 °C and the reaction mixture was

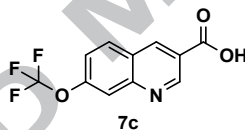
heated for fifteen hours. Upon cooling, the volatiles were removed in vacuo. The residue was dissolved in dichloromethane, washed with saturated sodium bicarbonate and brine, dried over sodium sulfate and concentrated. The residue was purified by flash chromatography, eluting with ethyl acetate:hexanes (1:49 to 1:1) to afford ethyl 4-chloro-7-(trifluoromethoxy)quinoline-3-carboxylate **5a** (2.72 g, 8.51 mmol, 32.8 % yield) as a waxy yellow solid. ^1H NMR (400 MHz, CDCl_3) δ 9.25 (s, 1H), 8.48 (d, 1H, $J = 9$ Hz), 7.98 (dq, 1H, $J = 2, 1$ Hz), 7.56 (dq, 1H, $J = 9, 2$ Hz), 4.52 (q, 2H, $J = 7$ Hz), 1.48 (t, 3H, $J = 7$ Hz); LC-MS (LC-ES) $\text{M}+\text{H} = 320$.

Ethyl 7-(trifluoromethoxy)quinoline-3-carboxylate **6a**



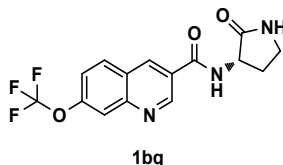
Bis(triphenylphosphine)palladium(II) dichloride (0.296 g, 0.422 mmol) was added to ethyl 4-chloro-7-(trifluoromethoxy)quinoline-3-carboxylate **5a** (2.70 g, 8.45 mmol) in acetonitrile (24 mL) and the reaction mixture was degassed for fifteen minutes by sparging with nitrogen. Triethylsilane (1.637 mL, 10.14 mmol) was added via syringe and the reaction mixture was heated in a sealed tube at 80 °C for nineteen hours. Upon cooling, the volatiles were removed in vacuo. The residue was taken up in ethyl acetate, filtered through Celite[®], washed with saturated sodium bicarbonate, water, and saturated sodium chloride, dried over sodium sulfate, and concentrated. The residue was purified by flash chromatography, eluting with ethyl acetate:hexanes (1:49 to 1:4) to afford ethyl 7-(trifluoromethoxy)quinoline-3-carboxylate **6a** (2.075 g, 7.28 mmol, 86 % yield) as a faintly yellow solid. ^1H NMR (400 MHz, CDCl_3) δ 9.49 (d, 1H, $J = 2$ Hz), 8.86 (d, 1H, $J = 2$ Hz), 8.01 (s, 1H), 8.00 (d, 1H, $J = 9$ Hz), 7.49 (dd, 1H, $J = 9, 2$ Hz), 4.50 (q, 2H, $J = 7$ Hz), 1.48 (t, 3H, $J = 7$ Hz); LC-MS (LC-ES) $\text{M}+\text{H} = 286$.

7-(Trifluoromethoxy)quinoline-3-carboxylic acid **7c**



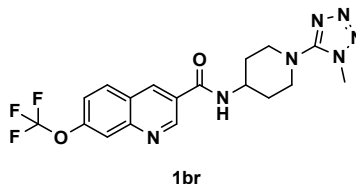
Lithium hydroxide monohydrate (1.515 g, 36.1 mmol) was added to a solution of ethyl 7-(trifluoromethoxy)quinoline-3-carboxylate **6a** (2.06 g, 7.22 mmol) in tetrahydrofuran (10 mL) and water (2 mL) and the reaction mixture was stirred at 60 °C for one hour. Upon cooling, the reaction mixture was poured into water (100 mL) and extracted with diethyl ether (1X). The aqueous layer was acidified by addition of 1 M hydrochloric acid (36 mL) and the precipitated solids were collected by filtration, washed with water, and air dried on the Buchner funnel. Then, further drying in a vacuum oven (50 °C / 25" Hg) afforded 7-(trifluoromethoxy)quinoline-3-carboxylic acid **7c** (1.79 g, 6.96 mmol, 96 % yield) as a colorless solid. ^1H NMR (400 MHz, CD_3SOCD_3) δ 13.67 (br s, 1H), 9.37 (d, 1H, $J = 2$ Hz), 9.07 (dd, 1H, $J = 2, 1$ Hz), 8.39 (d, 1H, $J = 9$ Hz), 8.01 (br s, 1H), 7.74 (ddd, 1H, $J = 9, 2, 1$ Hz); LC-MS (LC-ES) $\text{M}+\text{H} = 258$.

(S)-N-(2-Oxopyrrolidin-3-yl)-7-(trifluoromethoxy)quinoline-3-carboxamide **1bq**



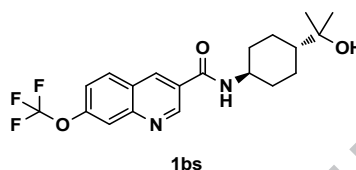
Method B; 7-(Trifluoromethoxy)quinoline-3-carboxylic acid **7c**; (S)-3-Amino-2-pyrrolidinone **8ao** (Biofine); *N,N*-Dimethylformamide; 8% yield; ^1H NMR (400 MHz, CD_3OD) δ 9.33 (d, 1H, $J = 2$ Hz), 8.86 (d, 1H, $J = 2$ Hz), 8.42 (br s, 1H), 8.18 (d, 1H, $J = 9$ Hz), 7.94 (br s, 1H), 7.62 (dd, 1H, $J = 9, 2$ Hz), 4.84-4.74 (m, 1H), 3.50-3.38 (m, 2H), 2.66-2.56 (m, 1H), 2.28-2.16 (m, 1H); LC-MS (LC-ES) $\text{M}+\text{H} = 340$.

N-(1-(1-methyl-1*H*-tetrazol-5-yl)piperidin-4-yl)-7-(trifluoromethoxy)quinoline-3-carboxamide **1br**



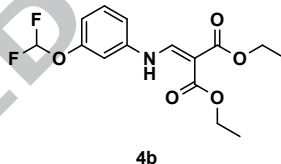
Method B; 7-(Trifluoromethoxy)quinoline-3-carboxylic acid **7c**; 1-(1-Methyl-1H-tetrazol-5-yl)piperidin-4-amine hydrochloride **8az** (Enamine); *N,N*-Dimethylformamide; 81% yield; ¹H NMR (400 MHz, CD₃SOCD₃) δ 9.35 (d, 1H, *J* = 2 Hz), 8.93 (d, 1H, *J* = 2 Hz), 8.81 (d, 1H, *J* = 8 Hz), 8.29 (d, 1H, *J* = 9 Hz), 8.01 (s, 1H), 7.72 (ddd, 1H, *J* = 9, 2, 1 Hz), 4.22-4.08 (m, 1H), 3.90 (s, 3H), 3.67 (d, 2H, *J* = 13 Hz), 3.16 (dt, 2H, *J* = 13, 2 Hz), 1.96 (dd, 2H, *J* = 13, 3 Hz), 1.78 (dq, 2H, *J* = 13, 3 Hz); LC-MS (LC-ES) M+H = 422.

***N*-(trans-4-(2-hydroxypropan-2-yl)cyclohexyl)-7-(trifluoromethoxy)quinoline-3-carboxamide 1bs.**



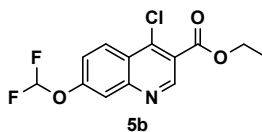
Method B; 7-(Trifluoromethoxy)quinoline-3-carboxylic acid **7c**; 2-(trans-4-Aminocyclohexyl)propan-2-ol **8bb** (PharmaBlock); *N,N*-Dimethylformamide; 86% yield; ¹H NMR (400 MHz, CD₃SOCD₃) δ 9.33 (d, 1H, *J* = 2 Hz), 8.90 (d, 1H, *J* = 2 Hz), 8.64 (d, 1H, *J* = 8 Hz), 8.28 (d, 1H, *J* = 9 Hz), 8.00 (s, 1H), 7.71 (ddd, 1H, *J* = 9, 2, 1 Hz), 4.07 (s, 1H), 3.77 (dt, 1H, *J* = 12, 8, 4 Hz), 1.96 (br d, 2H, *J* = 13 Hz), 1.85 (br d, 2H, *J* = 11 Hz), 1.33 (q, 2H, *J* = 12 Hz), 1.26-1.06 (m, 3H), 1.05 (s, 6H); LC-MS (LC-ES) M+H = 397.

Diethyl 2-(((3-(difluoromethoxy)phenyl)amino)methylene)malonate 4b.



A mixture of 3-(difluoromethoxy)aniline **2b** (2.04 g, 12.8 mmol) and diethyl 2-(ethoxymethylene)malonate **3** (2.77 g, 12.8 mmol) in ethanol (50 mL) was heated at reflux for 3 hours. The cooled mixture was evaporated to dryness to afford diethyl 2-(((3-(difluoromethoxy)phenyl)amino)methylene)malonate **4b** (4.2 g, 99% yield). LC-MS (LC-ES) M+H = 330.

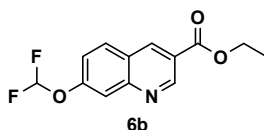
Ethyl 4-chloro-7-(difluoromethoxy)quinoline-3-carboxylate 5b.



A mixture of diethyl 2-(((3-(difluoromethoxy)phenyl)amino)methylene)malonate **4b** (4.2 g, 12.8 mmol) and phosphorus oxychloride (10 mL, 107 mmol) was heated in a sealed vial by microwave at 150 °C for 30 minutes. The cooled mixture was evaporated to dryness and the residue was taken up in dichloromethane (150 mL). The solution was treated cautiously with water (150 mL) and the aqueous phase was adjusted to pH = ~7 by the addition of 2 M aqueous sodium hydroxide solution. The organic phase was collected and the aqueous phase was extracted with additional dichloromethane (100 mL). The combined organics were evaporated to dryness and the product was purified by silica gel chromatography, eluting with ethyl acetate:cyclohexane (0:1 to 1:1) to afford ethyl 4-chloro-7-(difluoromethoxy)quinoline-3-carboxylate **5b** (1.2 g, 31% yield). ¹H NMR (400 MHz, CDCl₃) δ 9.23 (s, 1H), 8.45

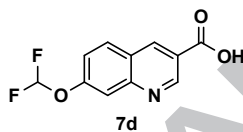
(d, 1H, $J = 9$ Hz), 7.81 (d, 1H, $J = 2$ Hz), 7.50 (dd, 1H, $J = 9, 2$ Hz), 6.75 (t, 1H, $J = 73$ Hz), 4.51 (q, 2H, $J = 7$ Hz), 1.48 (t, 3H, $J = 7$ Hz); LC-MS (LC-ES) $M+H = 302$.

Ethyl 7-(difluoromethoxy)quinoline-3-carboxylate **6b**.



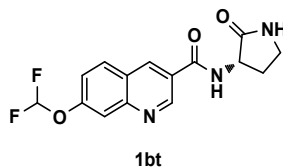
A mixture of ethyl 4-chloro-7-(difluoromethoxy)quinoline-3-carboxylate **5b** (1.1 g, 3.65 mmol) and triethylamine (2 mL, 14.4 mmol) in ethanol (120 mL) was added to palladium on carbon (Degussa type, 10 % wt) (110 mg) and stirred vigorously under an atmosphere of hydrogen for 1 hour. The reaction mixture was filtered through Celite® and then evaporated to dryness. The residue was purified by silica gel chromatography, eluting with ethyl acetate:cyclohexane (0:1 to 1:3) to afford ethyl 7-(difluoromethoxy)quinoline-3-carboxylate **6b** (910 mg, 93% yield). ^1H NMR (400 MHz, CDCl_3) δ 9.46 (s, 1H), 8.83 (d, 1H, $J = 2$ Hz), 7.96 (d, 1H, $J = 9$ Hz), 7.82 (br s, 1H), 7.42 (dd, 1H, $J = 9, 2$ Hz), 6.75 (t, 1H, $J = 73$ Hz), 4.49 (q, 2H, $J = 7$ Hz), 1.48 (t, 3H, $J = 7$ Hz); LC-MS (LC-ES) $M+H = 268$.

7-(Difluoromethoxy)quinoline-3-carboxylic acid **7d**.



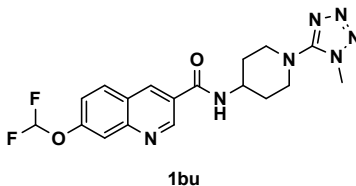
A suspension of ethyl 7-(difluoromethoxy)quinoline-3-carboxylate **6b** (870 mg, 3.26 mmol) in methanol (10 mL) was treated with a solution of sodium hydroxide (0.197 g, 4.93 mmol) in water (3 mL) and the mixture was heated at 50 °C for 1 hour. The cooled mixture was evaporated to dryness and the residue was taken up in water (60 mL) and acidified to pH 6 with 2 M aqueous hydrochloric acid. The precipitated product was filtered off, washed with water and dried in vacuo to afford 7-(difluoromethoxy)quinoline-3-carboxylic acid **7d** (655 mg, 56% yield). ^1H NMR (400 MHz, CD_3SOCD_3) δ 9.33 (d, 1H, $J = 2$ Hz), 8.99 (d, 1H, $J = 2$ Hz), 8.29 (d, 1H, $J = 9$ Hz), 7.79 (d, 1H, $J = 2$ Hz), 7.76 (t, 1H, $J = 73$ Hz), 7.35 (dd, 1H, $J = 9, 2$ Hz); LC-MS (LC-ES) $M+H = 240$.

(S)-7-(Difluoromethoxy)-*N*-(2-oxopyrrolidin-3-yl)quinoline-3-carboxamide **1bt**.



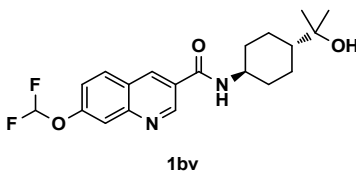
Method B; 7-(Difluoromethoxy)quinoline-3-carboxylic acid **7d**; (S)-3-Amino-2-pyrrolidinone **8ao** (Biofine); *N,N*-Dimethylformamide; 55% yield; ^1H NMR (400 MHz, CD_3SOCD_3) δ 9.33 (d, 1H, $J = 2$ Hz), 9.05 (d, 1H, $J = 8$ Hz), 8.89 (d, 1H, $J = 2$ Hz), 8.21 (d, 1H, $J = 9$ Hz), 7.90 (s, 1H), 7.79 (d, 1H, $J = 2$ Hz), 7.75 (t, 1H, $J = 73$ Hz), 7.54 (dd, 1H, $J = 9, 2$ Hz), 4.63 (dt, 1H, $J = 9, 7$ Hz), 3.34-3.22 (m, 2H), 2.46-2.36 (m, 1H), 2.12-1.98 (m, 1H); LC-MS (LC-ES) $M+H = 322$.

7-(Difluoromethoxy)-*N*-(1-(1-methyl-1*H*-tetrazol-5-yl)piperidin-4-yl)quinoline-3-carboxamide **1bu**.



Method B; 7-(Difluoromethoxy)quinoline-3-carboxylic acid **7d**; 1-(1-Methyl-1*H*-tetrazol-5-yl)piperidin-4-amine hydrochloride **8az** (Enamine); *N,N*-Dimethylformamide; 34% yield; ¹H NMR (400 MHz, CD₃SOCD₃) δ 9.31 (d, 1H, *J* = 2 Hz), 8.86 (s, 1H), 8.72 (d, 1H, *J* = 8 Hz), 8.20 (d, 1H, *J* = 9 Hz), 7.78 (s, 1H), 7.75-7.35 (m, 2H), 4.20-4.06 (m, 1H), 3.88 (s, 3H), 3.67 (d, 2H, *J* = 13 Hz), 3.16 (t, 2H, *J* = 13 Hz), 1.96 (d, 2H, *J* = 13 Hz), 1.78 (dq, 2H, *J* = 13, 3 Hz); LC-MS (LC-ES) M+H = 404.

7-(Difluoromethoxy)-*N*-((trans)-4-(2-hydroxypropan-2-yl)cyclohexyl)quinoline-3-carboxamide 1bv.



Method B; 7-(Difluoromethoxy)quinoline-3-carboxylic acid **7d**; 2-(trans-4-Aminocyclohexyl)propan-2-ol **8bb** (PharmaBlock); *N,N*-Dimethylformamide; 60% yield; ¹H NMR (400 MHz, CD₃SOCD₃) δ 9.29 (d, 1H, *J* = 2 Hz), 8.83 (d, 1H, *J* = 2 Hz), 8.55 (d, 1H, *J* = 8 Hz), 8.19 (d, 1H, *J* = 9 Hz), 7.78 (d, 1H, *J* = 2 Hz), 7.54 (t, 1H, *J* = 73 Hz), 7.52 (dd, 1H, *J* = 9, 2 Hz), 4.04 (s, 1H), 3.80-3.66 (m, 1H), 1.97 (br d, 2H, *J* = 10 Hz), 1.87 (br d, 2H, *J* = 12 Hz), 1.30 (br q, 2H, *J* = 12 Hz), 1.24-1.08 (m, 3H), 1.07 (s, 6H); LC-MS (LC-ES) M+H = 379.

H-PGDS RapidFire™ High Throughput Mass Spectrometry Assay. The H-PGDS RapidFire™ mass spectrometric assay monitors conversion of prostaglandin H₂ (PGH₂) to prostaglandin D₂ (PGD₂) by haematopoietic prostaglandin D synthase (H-PGDS). In the assay format described here, the substrate (PGH₂) is formed in situ by the action of cyclooxygenase-2 on arachidonic acid. This first step is set up to be fast, and generates a burst of PGH₂ at ~10 μM. The PGH₂ is then further converted to PGD₂ by the H-PGDS enzyme. The reaction is quenched with tin (II) chloride in citric acid, which converts any remaining PGH₂ to the more stable PGF_{2α}. Plates are then read on the RapidFire™ high throughput solid phase extraction system (Agilent) which incorporates a solid phase extraction step coupled to a triple quadrupole mass spectrometer (AB SCIEX). Relative levels of PGD₂ and PGF_{2α}, which acts as a surrogate for substrate, are measured and a percent conversion calculated. Inhibitors are characterized as compounds which lower the conversion of PGH₂ to PGD₂.

Expression and purification of H-PGDS protein. Full length human H-PGDS cDNA (Invitrogen Ultimate ORF IOH13026) was amplified by PCR with the addition of a 5' 6-His tag and TEV protease cleavage site. The PCR product was digested with NdeI and XhoI and ligated into pET22b+ (Merck Novagen®). Expression was carried out in *E. coli* strain BL21 (DE3*) using auto-induction Overnight Express™ Instant TB medium (Merck Novagen®) supplemented with 1 % glycerol. The culture was first grown at 37 °C and the temperature was reduced to 25 °C when OD600 reached 2.0. Cells were harvested by centrifugation after a further 18 hours. 10 g of *E. coli* cell pellet was suspended to a total volume of 80 mL in lysis buffer (20 mM Tris-Cl pH 7.5, 300 mM NaCl, 20 mM imidazole, 5 mM β-mercaptoethanol, 10 % glycerol). 1 mg/mL protease inhibitors (Protease Inhibitor Cocktail Set III, Merck Calbiochem®) and 1 mg/mL lysozyme were added to the cell suspension. The suspension was then sonicated for 5 minutes (UltraSonic Processor VCX 750, Cole-Parmer Instrument Co.) with a micro probe (50 % amplitude, 10 second on/off) and then centrifuged at 100,000 g for 90 minutes (at 4 °C). The supernatant was loaded onto a Ni-NTA HiTrap® column (5 mL, GE Healthcare, pre-equilibrated in lysis buffer). The column was washed with 10 column volumes of lysis buffer and eluted with lysis buffer containing 500 mM imidazole. The pooled protein peak fractions were concentrated using a 10 kDa centrifugal filter at 3500 g and 4 °C (Amicon Ultra-15 centrifugal filter unit with Ultracel-10 membrane from Millipore). Further purification of the concentrated protein was carried out using gel filtration chromatography on a HiLoad® 26/600 Superdex™ 75 preparative grade column (GE Healthcare Life Sciences) using 50 mM Tris pH 7.5, 50 mM NaCl, 1 mM dithiothreitol, 1 mM MgCl₂. Fractions containing the protein were pooled, concentrated as described above, and stored at -80 °C. For protein used in crystallography, the 6-His tag was removed with TEV protease prior to the gel filtration step.

Expression and purification of cyclooxygenase-2 (COX-2) protein. The full length human COX-2 gene (accession number L15326) was amplified by PCR to generate an EcoRI – HindIII fragment containing an in-frame FLAG tag. This was subcloned into pFastBac 1 (Invitrogen). The COX-2 FLAG plasmid was recombined into the baculovirus genome according to the BAC-to-BAC protocol described by Invitrogen. Transfection into *Spodoptera frugiperda* (Sf9) insect cells was performed using Cellfectin® (Invitrogen), according to the manufacturer's protocol. Super Sf9

cells were cultured in EX420 media (SAFC Biosciences) to a density of approximately 1.5×10^6 cells/mL within a wave bioreactor. Recombinant virus was added at a Multiplicity of Infection (MOI) of 5 and the culture was allowed to continue for 3 days. Cells were harvested using a continuous feed centrifuge run at 2500 g at a rate of approximately 2 L/min with cooling. The resultant cell slurry was re-centrifuged in pots (2500 g, 20 min, 4 °C) and the cell paste was stored at -80 °C. 342 g of cell paste was re-suspended to a final volume of 1600 mL in a buffer of 20 mM Tris-Cl pH 7.4, 150 mM NaCl, 0.1 mM EDTA, 1.3 % w/v n-octyl- β -D-glucopyranoside containing 20 Complete EDTA-free Protease Inhibitor Cocktail tablets (Roche Applied Science). The suspension was sonicated in 500 mL batches for 8 x 5 seconds at 10 u amplitude with the medium tip of an MSE probe sonicator and subsequently incubated at 4 °C for 90 minutes with gentle stirring. The lysate was centrifuged at 12000 rpm for 45 minutes at 4 °C in a Sorvall SLA1500 rotor. The supernatant (1400 mL) was added to 420 mL of 20 mM Tris-Cl pH 7.4, 150 mM NaCl, 0.1 mM EDTA to reduce the concentration of n-octyl- β -D-glucopyranoside to 1% w/v. The diluted supernatant was incubated overnight at 4 °C on a roller with 150 mL of anti-FLAG M2 agarose affinity gel (Aldrich-Sigma) which had been pre-equilibrated with 20 mM Tris-Cl pH 7.4, 150 mM NaCl, 0.1 mM EDTA, 1 % w/v n-octyl- β -D-glucopyranoside (purification buffer). The anti-Flag M2 agarose beads were pelleted by centrifugation in 500 mL conical Corning centrifuge pots at 2000 rpm for 10 min at 4 °C in a Sorvall RC3 swing-out rotor. The supernatant (unbound fraction) was discarded and the beads were re-suspended to half the original volume in purification buffer and re-centrifuged as above. The beads were then packed into a BioRad Econo Column (5 cm diameter) and washed with 1500 mL of purification buffer at 4 °C. Bound proteins were eluted with 100 μ g/mL triple FLAG peptide (Aldrich-Sigma) in purification buffer. Six fractions each of 0.5 column volume were collected. After each 0.5 column volume of purification buffer was added into the column the flow was held for 10 minutes before elution. Fractions containing COX-2 were pooled resulting in a protein concentration of ~ 1 mg/mL. The protein was further concentrated on Vivaspin 20 centrifugal concentrators (10 kDa cut-off) to 2.4 mg/mL and then stored at -80 °C.

Test compound plate preparation. Test compounds were diluted to 1 mM in DMSO and a 1:3, 11 point serial dilution was performed across a 384 well HiBase plate (Greiner Bio-one). 100 nL of this dilution series was then transferred into a 384 well v-base plate (Greiner Bio-one) using an EchoTM acoustic dispenser (Labcyte Inc) to create the assay plate. 100 nL of DMSO was added to each well in columns 6 and 18 for use as control columns.

Assay Method. 5 μ L of an enzyme solution containing 10 nM H-PGDS enzyme, 1.1 μ M COX-2 enzyme (COX-1 may be substituted for COX-2 in the assay, but the assay would then need to be reoptimized to determine appropriate reagent amounts, conditions, etc., for optimum production of PGH₂ from arachidonic acid) and 2 mM reduced glutathione (Sigma-Aldrich), diluted in a buffer of 50 mM Tris-Cl pH 7.4, 10 mM MgCl₂ and 0.1 % Pluronic F-127 (all Sigma-Aldrich) was added to each well of the plate except column 18 using a Multidrop Combi[®] dispenser (Thermo Fisher Scientific). 5 μ L of enzyme solution without H-PGDS was added to each well in column 18 of the assay plate to generate 100 % inhibition control wells.

Immediately after the addition of enzyme solution, 2.5 μ L of a co-factor solution containing 4 μ M Hemin (Sigma-Aldrich) diluted in buffer of 50 mM Tris-Cl pH 7.4 and 10 mM MgCl₂ (all Sigma-Aldrich), was added to each well using a Multidrop Combi[®] dispenser. 2.5 μ L of substrate solution containing 80 μ M arachidonic acid (Sigma-Aldrich) and 1 mM sodium hydroxide (Sigma-Aldrich) diluted in HPLC grade water (Sigma-Aldrich) was then added to each well using a Multidrop Combi[®] dispenser, to initiate the reaction.

The assay plates were incubated at room temperature for the duration of the linear phase of the reaction (usually 1 min 30 s – 2 min, this timing should be checked on a regular basis). Precisely after this time, the reaction was quenched by the addition of 30 μ L of quench solution containing 32.5 mM SnCl₂ (Sigma-Aldrich) in 200 mM citric acid (adjusted to pH 3.0 with 0.1 mM NaOH solution) to all wells using a Multidrop Combi[®] dispenser (Thermo Fisher Scientific). The SnCl₂ was initially prepared as a suspension at an equivalent of 600 mM in HPLC water (Sigma-Aldrich) and sufficient concentrated hydrochloric acid (Sigma-Aldrich) was added in small volumes until dissolved. The assay plates were centrifuged at 1000 rpm for 5 min prior to analysis.

The assay plates were analyzed using a RapidFireTM high throughput solid phase extraction system (Agilent) coupled to a triple quadrupole mass spectrometer (AB SCIEX) to measure relative peak areas of PGF_{2 α} and PGD₂ product. Peaks were integrated using the RapidFireTM integrator software before percentage conversion of substrate to PGD₂ product was calculated as shown below:

$$\% \text{ Conversion} = ((\text{PGD}_2 \text{ peak area}) / (\text{PGD}_2 \text{ peak area} + \text{PGF}_{2\alpha} \text{ peak area})) \times 100.$$

Data were further analyzed within ActivityBase software (IDBS) using a four parameter curve fit of the following form:

$$y = \frac{a - d}{1 + \left(\frac{x}{c}\right)^b} + d$$

where a is the minimum, b is the Hill slope, c is the IC₅₀ and d is the maximum. Data are presented as the mean IC₅₀.

H-PGDS Rat Basophilic Leukemia (RBL) cell inhibition assay. The cellular assay used for measuring inhibition of H-PGDS employed a rat model for testing compounds for inhibition of PGD₂ production. PGD₂ signal is generated through rat basophil leukemia (RBL) cells. These cells are adherent and will produce PGD₂ upon the addition of A23187 (Calcimycin, a calcium ionophore).

RBL cells were grown within T175 flasks for up to 15 passages. The cells were detached and plated into 96 well assay plates at a density of 5e⁴ cells/well in 100 μL/well. After 30 minutes of equilibration at room temperature, the plated cells were allowed to sit in a 37 °C, 5% CO₂ incubator overnight. On the day of processing, compounds were serially diluted with a top concentration of 5e⁵ [M] for 10 doses at a 1:3 dilution scheme. The compounds were stamped into each plate at 2 μL/well and were diluted with 38 μL of HBSS. The next day, the cells had attached themselves to the bottom of the wells and were ready to be washed. (Washing the cells was performed due to the 10% FBS within the growth media.) After 3 x 160 μL washes with HBSS, 160 μL of HBSS was left in the well and 20 μL (out of the 40 μL) of compounds were transferred into the wells of the washed cells (160 μL HBSS/cells + 20 μL compd). The compound and cells were incubated together for 30 minutes at 37 °C/5% CO₂. After the incubation, the compound and cells had 20 μL of A23187 added into the assay plate (180 μL HBSS/cells/compd + 20 μL A23187). The compound, cells and ionophore were incubated together for 30 minutes at 37 °C/5% CO₂. At the 25 minute mark, the assay plates were removed from the incubator and spun in the centrifuge for 5 minutes at 1000 rpms. The assay was then quenched by transferring 90 μL (out of 200 μL) of supernatant into 40 μL of acetonitrile with 20 ng/mL PGD₂-d₄ (internal standard).

The completed assay plate was then sampled and read on the RapidFire Mass Spectrometer (RF-MS). Samples could also be frozen (at -20 °C) for about 2 weeks before signal degrades. The RF-MS was tuned to capture the PGD₂ product at xic 351.2/271.2 and the PGD₂-d₄ spiked in product at xic 355.2/275.1 on a Agilent 4000 or 5500.

L-PGDS RapidFire™ High Throughput Mass Spectrometry Assay. This protocol describes an assay to measure conversion of PGH₂ to PGD₂ by lipocalin prostaglandin D synthase (L-PGDS) using high throughput mass spectrometry. In the assay format described here, the substrate (PGH₂) is obtained commercially. The PGH₂ is converted to PGD₂ by the L-PGDS enzyme. There is also non-PGDS dependent conversion of PGH₂ to PGD₂, and this conversion is accounted for in control wells of the assay plate where no L-PGDS is added. The assay is tuned to achieve approximately 25-30% conversion of the PGH₂ that is L-PGDS-dependent. The reaction is quenched in all wells with tin (II) chloride which converts any remaining PGH₂ to the more stable PGF_{2α}. Plates are then analyzed on the RapidFire™ system (Agilent) which incorporates a solid phase extraction step coupled to an electrospray ionization triple quadrupole mass spectrometer (AB SCIEX). Relative levels of PGD₂ and PGF_{2α}, which acts as a surrogate to substrate, are measured and a percent conversion calculated. Inhibitors are characterized as compounds which lower the conversion of PGH₂ to PGD₂. The data analysis was similar to the H-PGDS RapidFire™ assay above.

mPGES RapidFire™ High Throughput Mass Spectrometry Assay. This protocol describes a functional assay to measure conversion of PGH₂ to PGE₂ by mPGES using high throughput mass spectrometry. In the assay format described here, the substrate (PGH₂) is formed in situ by the action of cyclooxygenase-2 on arachidonic acid. This first step is set up to be fast, and generates a burst of PGH₂ at ~10-20 μM (~K_m of PGH₂ for mPGES-1). The reaction is quenched with tin (II) chloride, which converts any remaining PGH₂ to the more stable PGF_{2α}. Plates are then analyzed on the RapidFire™ system, which incorporates a solid phase extraction step coupled to an electrospray ionization triple quadrupole mass spectrometer. Relative levels of PGE₂ and PGF_{2α}, which acts as a surrogate to substrate, are measured and a percent conversion calculated. Inhibitors are characterized as compounds which lower the conversion of PGH₂ to PGE₂. The data analysis was similar to the H-PGDS RapidFire™ assay above.

Artificial Membrane Permeability (AMP) assay. Add 3.5 μL of 1.8% lipid (L- α -phosphatidylcholine) in 1% cholesterol decane solution to the filter plate, shake the plate for 12 seconds, and then add 250 μL of buffer (50 mM phosphate buffer with 0.5% hydroxypropyl-cyclodextrin (encapsin), pH at 7.4) to donor side and 100 μL to the receiver side. The assay plate is shaken for 45 minutes before adding the compounds. Add the compounds (2.5 μL) to the donor side. The assay is run as replicates. Assay plate 1 and 2 test the sample plate 1; assay plate 3 and 4 test the sample plate 2. The assay plates are then incubated at room temperature on the shaker for 3 hours. Transfer the assay samples to the HPLC analysis plates. Aspirate 100 μL of receiver solution and transfer them to the receiver analysis plate, then transfer 100 μL donor solution to the donor analysis plate. The AMP assay samples were analyzed by HPLC.

Mouse liver microsome assay. Dilute 10 mM dimethyl sulfoxide stock of new chemical entity (NCE) to an appropriate intermediate concentration such that the final test concentration in the incubation is 0.5 mM and final organic solvent content is limited to 0.25%. Thaw liver microsomes in a room temperature water bath and immediately place on ice until ready to use. Vortex the microsomes and dilute to appropriate concentration using 50 mM phosphate buffer, pH 7.4. Add diluted NCE (0.5 mM final NCE concentration). Add diluted microsomes (0.5 mg/mL final protein concentration). Pre-incubate the plate for 5 minutes at 37 $^{\circ}\text{C}$ with shaking before adding cofactor solution (Final concentration in the incubation system: β -nicotinamide adenine dinucleotide phosphate (0.44 mM); glucose 6-phosphate (5.2 mM); glucose-6-phosphate dehydrogenase (1.2 U/mL); sodium bicarbonate (0.4%); 5 mM magnesium chloride or 1 mM nicotinamide adenine dinucleotide phosphate). Start the reaction by adding prewarmed (37 $^{\circ}\text{C}$) cofactor solution. Mix the reaction for \sim 30 seconds. Remove a fixed volume of microsomal incubation (e.g. 100 μL) at 6 timepoints up to 45 minutes and place into a 96-deepwell plate containing 2 volumes of chilled acetonitrile (e.g. 200 μL) containing Internal standard; reaction plate should be maintained at 37 $^{\circ}\text{C}$ with shaking during the entire incubation period. Precipitate protein by mixing and centrifugation (2000 \times g, 15 minutes). Transfer resultant supernatant to a new 96-well plate for LC-MS/MS analysis. Metabolic stability expressed as the percentage of parent NCE remaining is calculated from the peak area of NCE remaining after incubation (t_x) compared to the time zero (t_0) incubation. The half-life ($t_{1/2}$) is calculated using the following equation: $t_{1/2} = -\ln(2)/k$, where k is the turn-over rate constant of the \ln % remaining vs. time regression. Intrinsic Clearance (C_{rnt}) is calculated from the half-life using the following equations:

$$C_{\text{rnt}} = (0.693/ t_{1/2} \text{ min}) \times (\text{mL of incubation/mg microsomal protein}) \times (\text{mg microsomal protein/gm liver}) \times (\text{gm liver/kg body wt}).$$

Constant used for mg microsomal protein/gm liver: (46-rat, 48-mouse, 36.7-dog, 39.7- human, 52.5-monkey, 52.5-minipig). Constants used to represent gm/liver/kg body weight: (36-rat, 51-mouse, 32.5-dog, 24.5- human, 30-monkey, 16.7-minipig).

Fasted State Simulated Intestinal Fluid Solubility (FaS-SIF) assay.

Simulated Intestinal Fluid Solution. Dissolve potassium phosphate monobasic (4.083 g) and potassium chloride (7.455 g) in water. Add 1.0 M sodium hydroxide (100 mL) and add water in a sufficient quantity to make 1 liter of Simulated Intestinal Fluid Buffer Solution. Then, dissolve 0.056 g of simulated intestinal fluid powder (Can be purchased or made from sodium taurocholate and lecithin) in 25 mL of Simulated Intestinal Fluid Buffer Solution.

Fasted State Simulated Intestinal Fluid Solubility (FaS-SIF) assay. Into a suitable container (eppendorf tube or glass screw cap vial) add drug substance (typically 1-5 mg). Wet the compound with physiologically relevant media (i.e. simulated intestinal fluid, simulated gastric fluid) (for solubilities between 0.1–500 $\mu\text{g/mL}$, plan on 10 mL per time point) by either sonication, shaking or vortex mixing and record any initial visual observations. Transfer to a mechanical shaker, roller mixer, or stir plate. Equilibrate at ambient temperature (\sim 21 – 23 $^{\circ}\text{C}$) or in a thermostatic water bath at 25 $^{\circ}\text{C}$. Establish equilibrium at two time points (4 and 24 hrs or 24 and 48 hrs). At each sample pull, the following should be recorded: Elapsed time, measured pH, and visual observations (color changes, absence of solid, etc). Filter the sample using syringe filters, then dispense filtrate into an HPLC vial. Inject an aliquot into the HPLC and compare area to standard to determine solubility.

Crystallization Conditions. Apo crystals were grown using the vapor diffusion method. Protein [\sim 10-26 mg/mL in 50 mM tris(hydroxymethyl)aminomethane hydrochloride at pH 7.5, 50 mM sodium chloride, 1 mM dithiothreitol, 15 mM glutathione, and 1 mM magnesium chloride] was mixed with an equal volume of precipitant solution (18% poly(ethylene glycol) 6000, 1.4% dioxane, 5% glycerol, 10 mM dithiothreitol, and 50 mM

tris(hydroxymethyl)aminomethane hydrochloride at pH 8.5 or 0.2 M sodium fluoride, 24.0% poly(ethylene glycol) 3350). Rod-like crystals formed in 3-7 days at room temperature and were soaked for ~4-24 hours with 0.5-25 mM inhibitor. X-ray diffraction data was collected on an RAXIS detector operating on a FRE+ generator or at the Advanced Photon Source (APS, Ser-CAT 22ID) using an Eiger detector. Data were integrated and processed using either D*Trek or HKL2000. The structures were solved by molecular replacement using MOLREP. The phases were refined using the CCP4 suite and manual rebuilding using Coot.

Mast Cell Degranulation Assay. Eleven-week-old C57BL/6J male mice were randomized by body weight into 7 treatment groups, then dosed (p.o.) with either vehicle or the H-PGDS inhibitor **1bv** at doses of 0.03, 0.1, 0.3, 1.0 and 3.0 mg/kg. One hour later, mice were anesthetized and injected (i.p.) with phosphate buffered saline (0.2 mL) or compound 48/80 solution (0.75 mg/ml, Sigma), followed by gentle massage of the abdomen. Mice were kept under anesthesia for 7 minutes before blood was collected by cardiac puncture for measurement of inhibitor concentration. Mice were then euthanized by cervical dislocation. The abdominal cavity was opened with a small incision and filled with phosphate buffered saline (2.0 mL) and the abdomen was gently massaged for several seconds. Lavage fluid (1 mL) was removed, spun down (12,000 rpm for 2 minutes) and the supernatant kept on dry ice and later used for measurement of PGD₂ levels using a PGD₂-MOX EIA kit.

1.6 Notes

Declarations of interest: The authors are employees of GlaxoSmithKline or Astex.

This research did not receive any specific grant from funding agencies in the public, commercial, or not-for-profit sectors.

1.7 Acknowledgements

The authors would like to thank Nathalie Barrett, Philip J. Day, Bernadette H. Mouzon, Vaughan Leyden, and David Taylor for the cloning, expression, and purification of the H-PGDS protein that was used in the biochemical assays.

1.8 Supplementary data

Supplementary data associated with this article can be found, in the online version

1.9 References

1. Smith, W. L.; Urade, Y.; Jakobsson, P.-J. Enzymes of the cyclooxygenase pathways of prostanoid biosynthesis *Chem. Rev.* **2011**, *111*, 5821-5865.
2. Reid, G.; Wielinga, P.; Zelcer, N.; van der Heijden, I.; Kuil, A.; de Haas, M.; Wijnholds, J.; Borst, P. The human multidrug resistance protein MRP4 functions as a prostaglandin efflux transporter and is inhibited by nonsteroidal antiinflammatory drugs. *Proc. Natl. Acad. Sci. U. S. A.* **2003**, *100*, 9244-9249.
3. Hirata, T.; Narumiya, S. Prostanoid receptors. *Chem. Rev.* **2011**, *111*, 6209-6230.
4. Nakanishi, T.; Tamai, I. Roles of organic anion transporting polypeptide 2A1 (OATP2A1/SLCO2A1) in regulating the pathophysiological actions of prostaglandins. *AAPS J* **2018**, *20*, 1-14.
5. Tai, H.-H.; Cho, H.; Tong, M.; Ding, Y. NAD⁺-linked 15-hydroxyprostaglandin dehydrogenase: Structure and biological functions. *Curr. Pharm. Des.* **2006**, *12*, 955-962.
6. Watanabe, K. Recent reports about enzymes related to the synthesis of prostaglandin (PG) F₂ (PGF₂α and 9α, 11β-PGF₂) *J. Biochem.* **2011**, *150*, 593-596.
7. Kupczyk, M.; Kuna, P. Targeting the PGD₂/CRTH2/DP₁ signaling pathway in asthma and allergic disease: Current status and future perspectives *Drugs* **2017**, *77*, 1281-1294.
8. Trivedi, S. G.; Newson, J.; Rajakariar, R.; Jacques, T. S.; Hannon, R.; Kanaoka, Y.; Eguchi, N.; Colville-Nash, P.; Gilroy, D. W. Essential role for hematopoietic prostaglandin D₂ synthase in the control of delayed type hypersensitivity *Proc. Natl. Acad. Sci. U. S. A.* **2006**, *103*, 5179-5184.
9. Kabashima, K.; Narumiya, S. The DP receptor, allergic inflammation and asthma *Prostaglandins Leukot. Essent. Fatty Acids* **2003**, *69*, 187-194.
10. Parson, H. K.; Harati, H.; Cooper, D.; Vinik, A. I. Role of prostaglandin D₂ and the autonomic nervous system in niacin-induced flushing *J. Diabetes* **2013**, *5*, 59-67.

11. Jandl, K.; Heinemann, A. The therapeutic potential of CRTH2/DP2 beyond allergy and asthma *Prostaglandins Other Lipid Mediators* **2017**, *133*, 42-48.
12. Xu, X.-G.; Chen, H.-D. Prostanoids and hair follicles: Implications for therapy of hair disorders *Acta Derm. Venereol.* **2018**, *98*, 318-323.
13. Garza, L. A.; Liu, Y.; Yang, Z.; Alagesan, B.; Lawson, J. A.; Norberg, S. M.; Loy, D. E.; Zhao, T.; Blatt, H. B.; Stanton, D. C.; Carrasco, L.; Ahluwalia, G.; Fischer, S. M.; FitzGerald, G. A.; Cotsarelis, G. Prostaglandin D₂ inhibits hair growth and is elevated in bald scalp of men with androgenetic alopecia *Sci. Trans. Med.* **2012**, *4*, 126ra34.
14. Flanagan, J. U.; Smythe, M. L. Sigma-class glutathione transferases, *Drug Metab. Rev.* **2011**, *43*, 194-214.
15. Sanchez, D.; Ganfornina, M. D.; Gutierrez, G.; Marin, A. Exon-intron structure and evolution of the lipocalin gene family. *Mol. Biol. Evol.* **2003**, *20*, 775-783.
16. Feng, X.; Ramsden, M. K.; Negri, J.; Baker, M. G.; Payne, S. C.; Borish, L.; Steinke, J. W. Eosinophil production of prostaglandin D₂ in patients with aspirin-exacerbated respiratory disease *J. Allergy Clin. Immunol.* **2016**, *138*, 1089-1097.
17. Hyo, S.; Kawata, R.; Kadoyama, K.; Eguchi, N.; Kubota, T.; Takenaka, H.; Urade Y. Expression of prostaglandin D₂ synthase in activated eosinophils in nasal polyps *Arch. Otolaryngol. Head Neck Surg.* **2007**, *133*, 693-700.
18. Mohri, I.; Taniike, M.; Taniguchi, H.; Kanekiyo, T.; Aritake, K.; Inui, T.; Fukumoto, N.; Eguchi, N.; Kushi, A.; Sasai, H.; Kanaoka, Y.; Ozono, K.; Narumiya, S.; Suzuki, K.; Urade, Y. Prostaglandin D₂-mediated microglia/astrocyte interaction enhances astrogliosis and demyelination in twitcher. *J. Neurosci.* **2006**, *26*, 4383-4393.
19. Nakagawa, T.; Takeuchi, A.; Kakiuchi, R.; Lee, T.; Yagi, M.; Awano, H.; Iijima, K.; Takeshima, Y.; Urade, Y.; Matsuo, M. A prostaglandin D₂ metabolite is elevated in the urine of Duchenne muscular dystrophy patients and increases further from 8 years old *Clin. Chim. Acta* **2013**, *423*, 10-14.
20. Pellefigues, C.; Dema, B.; Lamri, Y.; Saidoune, F.; Chavarot, N.; Lohéac, C.; Pacreau, E.; Dussiot, M.; Bidault, C.; Marquet, F.; Jablonski, M.; Chemouny, J. M.; Jouan, F.; Dossier, A.; Chauveheid, M.-P.; Gobert, D.; Papo, T.; Karasuyama, H.; Sacré, K.; Daugas, E.; Charles, N. Prostaglandin D₂ amplifies lupus disease through basophil accumulation in lymphoid organs *Nat. Commun.* **2018**, *9*, 725.
21. Aritake, K.; Kado, Y.; Inoue, T.; Miyano, M.; Urade, Y. Structural and functional characterization of HQL-79, an orally selective inhibitor of human hematopoietic prostaglandin D synthase *J. Biol. Chem.* **2006**, *281*, 15277-15286.
22. Hestekamp, T.; Barker, J.; Davenport, A.; Whittaker, M. Fragment based drug discovery using fluorescence correlation spectroscopy techniques: Challenges and solutions *Curr. Top. Med. Chem.* **2007**, *7*, 1582-1591.
23. Hohwy, M.; Spadola, L.; Lundquist, B.; Hawtin, P.; Dahmén, J.; Groth-Clausen, I.; Nilsson, E.; Persdotter, S.; von Wachenfeldt, K.; Folmer, R. H. A.; Edman, K. Novel prostaglandin D synthase inhibitors generated by fragment-based drug design *J. Med. Chem.* **2008**, *51*, 2178-2186.
24. Carron, C. P.; Trujillo, J. I.; Olson, K. L.; Huang, W.; Hamper, B. C.; Dice, T.; Neal, B. E.; Pelc, M. J.; Day, J. E.; Rohrer, D. C.; Kiefer, J. R.; Moon, J. B.; Schweitzer, B. A.; Blake, T. D.; Turner, S. R.; Woerndle, R.; Case, B. L.; Bono, C. P.; Dilworth, V. M.; Funckes-Shippy, C. L.; Hood, B. L.; Jerome, G. M.; Kornmeier, C. M.; Radabaugh, M. R.; Williams, M. L.; Davies, M. S.; Wegner, C. D.; Welsch, D. J.; Abraham, W. M.; Warren, C. J.; Dowty, M. E.; Hua, F.; Zutshi, A.; Yang, J. Z.; Thorarensen, A. Discovery of an oral potent selective inhibitor of hematopoietic prostaglandin D synthase (HPGDS) *ACS Med. Chem. Lett.* **2010**, *1*, 59-63.
25. Weiberth, F. J.; Yu, Y.; Subotkowski, W.; Pemberton, C. Demonstration on pilot-plant scale of the utility of 1,5,7-triazabicyclo[4.4.0]dec-5-ene (TBD) as a catalyst in the efficient amidation of an unactivated methyl ester *Org. Proc. Res. Devel.* **2012**, *16*, 1967-1969.
26. Thurairatnam, S. Hematopoietic prostaglandin D synthase inhibitors. *Prog. Med. Chem.* **2012**, *51*, 97-133.
27. Takeshita, E.; Komaki, H.; Shimizu-Motohashi, Y.; Ishiyama, A.; Sasaki, M.; Takeda, S. A phase I study of TAS-205 in patients with Duchenne muscular dystrophy. *Ann. Clin. Trans. Neurol.* **2018**, *5*, 1338-1349.
28. Aoki, S. New crystal of piperazine compound, and preparation thereof. **WO 2017047791 A1** 20170323; 2017.
29. Murray, C. W.; Rees, D. C. The rise of fragment-based drug discovery. *Nat. Chem.* **2009**, *1*, 187-192.
30. Davies, T. G.; Tickle, I. J. Fragment screening using X-ray crystallography, *Top. Curr. Chem.* **2012**, *317*, 33-59.
31. Saxty, G.; Norton, D.; Affleck, K.; Clapham, D.; Cleasby, A.; Coyle, J.; Day, P.; Frederickson, M.; Hancock, A.; Hobbs, H.; Hutchinson, J.; Le, J.; Leveridge, M.; McMenamin, R.; Mortenson, P.; Page, L.; Richardson,

- C.; Russell, L.; Sherriff, E.; Teague, S.; Uddin, S.; Hodgson, S. Identification of orally bioavailable small-molecule inhibitors of hematopoietic prostaglandin D₂ synthase using X-ray fragment based drug discovery *Med. Chem. Commun.* **2014**, *5*, 134-141.
32. Hopkins, A. L.; Groom, C. R.; Alex, A. Ligand efficiency: a useful metric for lead selection *Drug Disc. Today* **2004**, *9*, 430-431.
33. Fryer, R. I.; Zhang, P.; Rios, R. o; Gu, Z. Q.; Basile, A. S.; Skolnick, P. Structure-activity relationship studies at benzodiazepine receptor (BZR): a comparison of the substituent effects of pyrazoloquinolinone analogs *J. Med. Chem.* **1993**, *36*, 1669-1673.
34. Santangelo, F.; Casagrande, C.; Miragoli, C.; Vecchietti, V. Synthesis and positive inotropic effect of 1-alkyl- and 1-acyl-6,7-dimethoxy-3-dimethylamino-1,2,3,4-tetrahydroquinolines *Eur. J. Med. Chem.* **1994**, *29*, 877-882.
35. Irvine, J. D.; Takahashi, L.; Lockhart, K.; Cheong, J.; Tolan, J. W.; Selick, H. E.; Grove, J. R. MDCK (Madin-Darby canine kidney) cells: A tool for membrane permeability screening. *J. Pharm. Sci.* **1999**, *88*, 28-33.
36. Dressman, J. B.; Amidon, G. L.; Reppas, C.; Shah, V. P. Dissolution testing as a prognostic tool for oral drug absorption: immediate release dosage forms. *Pharm. Res.* **1998**, *15*, 11-22.
37. Jakobsson, P.-J.; Thorén, S.; Morgenstern, R.; Samuelsson, B. Identification of human prostaglandin E synthase: a microsomal glutathione-dependent, inducible enzyme, constituting a potential novel drug target. *Proc. Natl. Acad. Sci. U. S. A.* **1999**, *96*, 7220-7225.
38. Gillie, D. J.; Novick, S. J.; Donovan, B. T.; Payne, L. A.; Townsend, C. Development of a high-throughput electrophysiological assay for the human ether-a-go-go related potassium channel hERG. *J. Pharmacol. Toxicol. Methods* **2013**, *67*, 33-44.
39. Rothchild, A. M. Mechanisms of histamine release by compound 48/80 *Br. J. Pharmacol.* **1970**, *38*, 253-262.
40. Limberg, G.; Lundt, I.; Zavilla, J. Deoxyiminoalditols from aldonic acids VI. Preparation of the four stereoisomeric 4-amino-3-hydroxypyrrolidines from bromodeoxytetric acids. Discovery of a new α -mannosidase inhibitor *Synthesis* **1999**, *1*, 178-183.
41. Parsons, W. H. Lactams and bicyclic lactams useful as cholecystokinin antagonists **US 4757068** 19880712; 1988.
42. Cadilla, R.; Deaton, D. N.; Hancock, A. P.; Hobbs, H.; Hodgson, S. T.; Larkin, A. L.; Le, J.; Mortenson, P. N.; Price, D. J.; Saxty, G.; Schaller, L. T.; Schulte, C.; Smith, I. E. D.; Thomson, S. A.; Wilson, J. W. Quinoline-3-carboxamides as H-PGDS inhibitors. **WO 2017103851** A1 20170622; 2017.

Graphical Abstract

The discovery of quinoline-3-carboxamides as hematopoietic prostaglandin D synthase (H-PGDS) inhibitors

David N. Deaton,^{a,*} Young Do,^a Jason Holt,^a Michael R. Jeune,^a H. Fritz Kramer,^a Andrew L. Larkin,^a Lisa A. Orband-Miller,^a Gregory E. Peckham,^a Chuck Poole,^a Daniel J. Price,^a Lee T. Schaller,^a Ying Shen,^a Lisa M. Shewchuk,^a Eugene L. Stewart,^a J. Darren Stuart,^a Stephen A. Thomson,^a Paris Ward,^a Joseph W. Wilson,^a Tianshun Xu,^a Jeffrey H. Guss,^b Caterina Musetti,^b Alan R. Rendina,^b Karen Affleck,^c David Anders,^c Ashley P. Hancock,^c Heather Hobbs,^c Simon T. Hodgson,^c Jonathan Hutchinson,^c Melanie V. Leveridge,^c Harry Nicholls,^c Ian E. D. Smith,^c Don O. Somers,^c Helen F. Sneddon,^c Sorif Uddin,^c Anne Cleasby,^d Paul N. Mortenson,^d Caroline Richardson,^d Gordon Saxty,^d

^aGlaxoSmithKline, 5 Moore Drive, P.O. Box 13398, Research Triangle Park, NC 27709, USA

^bGlaxoSmithKline, 1250 South Collegeville Road, Collegeville, PA 19426, USA

^cGlaxoSmithKline, Gunnels Wood Road, Stevenage, Hertfordshire SG1 2NY, UK

^dAstex Pharmaceuticals, 436 Cambridge Science Park, Milton Road, Cambridge CB4 0QA, UK

